Atmosphere-Ocean
Publication details, including instructions for authors and subscription information:
http://www.tandfonline.com/loi/tato20

Sensitivity of climate simulations to the parameterization of cumulus convection in the Canadian climate centre general circulation model

G.J. Zhang [a] & Norman A. McFarlane [b]

[a] California Space Institute, Scripps Institution of Oceanography, University of California at San Diego, La Jolla, CA, 92093

[b] Canadian Centre for Climate Modelling and Analysis, University of Victoria, P.O. Box 1700 MS 3339, Victoria, B.C., V8W 2Y2, Canada

Published online: 19 Nov 2010.

To cite this article: G.J. Zhang & Norman A. McFarlane (1995): Sensitivity of climate simulations to the parameterization of cumulus convection in the Canadian climate centre general circulation model, Atmosphere-Ocean, 33:3, 407-446

To link to this article: http://dx.doi.org/10.1080/07055900.1995.9649539

Sensitivity of Climate Simulations to the Parameterization of Cumulus Convection in the Canadian Climate Centre General Circulation Model

G.J. Zhang
California Space Institute
Scripps Institution of Oceanography
University of California at San Diego
La Jolla CA 92093

and

Norman A. McFarlane
Canadian Centre for Climate Modelling and Analysis
University of Victoria
P.O. Box 1700 MS 3339
Victoria, B.C. V8W 2Y2, Canada

[Original manuscript received 15 April 1994; in revised form 14 November 1994]

ABSTRACT *A simplified cumulus parameterization scheme, suitable for use in GCMs, is presented. This parameterization is based on a plume ensemble concept similar to that originally proposed by Arakawa and Schubert (1974). However, it employs three assumptions which significantly simplify the formulation and implementation of the scheme. It is assumed that an ensemble of convective-scale updrafts with associated saturated downdrafts may exist when the atmosphere is locally conditionally unstable in the lower troposphere. However, the updraft ensemble is comprised only of those plumes which are sufficiently buoyant to penetrate through this unstable layer. It is assumed that all such plumes have the same upward mass flux at the base of the convective layer. The third assumption is that moist convection, which occurs only when there is convective available potential energy (CAPE) for reversible ascent of an undiluted parcel from the sub-cloud layer, acts to remove CAPE at an exponential rate with a specified adjustment time scale.*

The performance of the scheme and its sensitivity to choices of disposable parameters is illustrated by presenting results from a series of idealized single-column model tests. These tests demonstrate that the scheme permits establishment of a quasi-equilibrium between large-scale forcing and convective response. However, it is also shown that the strength of convective downdrafts is an important factor in determining the nature of the equilibrium state. Relatively strong down-drafts give rise to an unsteady irregularly fluctuating state characterized by alternate periods of deep and shallow convection.

The effect of using the scheme for GCM climate simulations is illustrated by presenting

ATMOSPHERE-OCEAN 33 (3) 1995, 407–446 0705-5900/95/0000-0407$01.25/0

selected results of a multi-year simulation carried out with the Canadian Climate Centre GCM using the new parameterization (the CONV simulation). Comparison of these results with those for a climate simulation made with the standard model (the CONTROL simulation, as documented by McFarlane et al., 1992) reveals the importance of other parameterized processes in determining the ultimate effect of introducing the new convective scheme. The radiative response to changes in the cloudiness regime is particularly important in this regard.

RÉSUMÉ *On présente un schéma simplifié de paramétrisation des Cumulus, utilisable dans les MCG. La paramétrisation est basée sur un concept de panache semblable à celui proposé par Arakawa et Schubert (1974). Toutefois, il utilise trois hypothèses qui simplifient significativement la formulation et la mise en oeuvre du schéma. On suppose qu'un ensemble de courants ascendants à l'échelle convective et les courants ascendants saturés associés sont possibles lorsque l'atmosphère est localement conditionnellement instable dans la basse troposphère. L'ensemble des courants ascendants ne comprend cependant que les panaches qui ont suffisamment de flottabilité pour pénétrer la couche instable. On suppose que tout panache semblable a le même flux de masse ascendant à la base de la couche convective. La troisième supposition est que la convection humide, présente seulement lorqu'il y a de l'énergie convective potentielle disponible (CAPE) pour une montée réversible d'une particule non diluée de la couche de bas nuages, enlève la CAPE à un taux exponentiel avec une échelle de temps spécifiquement ajustable.*

On illustre la performance du schéma et sa sensibilité aux choix de paramètres disposables en présentant les résultats d'une série de tests idéalisés de modèle à simple colonne. Ces tests montrent que le schéma permet d'établir un quasi équilibre entre le forçage à grande échelle et la réponse convective. Cependant, on montre aussi que la force des courants descendants convectifs est un facteur important pour déterminer la nature de l'état d'équilibre. Les courants descendants relativement forts entraînent un état fluctuant irrégulièrement instable caractérisé par des périodes alternées de convection profonde et mince.

On montre l'effet de l'utilisation du schéma dans les simulations climatiques du MCG en présentant des résultats sélectionnés d'une simulation de plusieurs années à l'aide du MCG du Centre climatologique canadien qui utilise les nouvelles paramétrisations (CONV). La comparaison de ces résultats avec ceux d'une simulation climatique produite par le modèle standard (simulation CONTROL documentée par McFarlane et al., 1992), montre l'importance de d'autres processus paramétrisés pour déterminer l'effet ultime de l'introduction du nouveau schéma convectif. À ce sujet, la réponse radiative aux changements dans le régime de nébulosité est particulièrement importante.

1 Introduction

It has been recognized for decades that the effects of cumulus clouds must be parameterized in numerical weather prediction and general circulation models. However, there is not a consensus regarding the representation of these effects in large-scale models. The parameterization schemes currently in use range in complexity from simple moist convective adjustment schemes that are similar to that proposed by Manabe et al. (1965) almost three decades ago to complicated mass flux schemes utilizing and elaborating the basic concepts set forth by Arakawa and Schubert (1974). These also include adaptations of the parameterization concepts of Kuo (1965, 1974) and in some cases (e.g., Tiedtke, 1989) the chosen parameterization scheme employs the mass flux approach while using moisture convergence closure

conditions as suggested by Kuo (1974). The validity of this closure approach has recently been questioned (Emanuel, 1991) and, in any event, is not required to ensure a close relationship between large-scale convergence and latent heat release due to moist convection. For example, Gregory and Rowntree (1990) show that such is the case for simulations made with their bulk cumulus parameterization scheme in which the initial upward mass flux is specified in terms of the parcel buoyancy in the lower part of the convective layer.

Recently Betts (1986) proposed an adjustment procedure based on the concept (supported to some extent by observations) that moist convection acts to relax the atmosphere toward a state in which the large-scale virtual temperature structure in the lower troposphere (below the freezing level) is close to that for a parcel undergoing reversible moist ascent. Since this reference state is not an unstable one, persistent convection requires that the tendency for convective processes to stabilize the atmosphere be balanced by the conteracting effects of other processes acting on larger scales. Such a quasi-equilibrium assumption is also a fundamental part of the Arakawa and Schubert (1974) parameterization scheme and is also utilized in a distinctly different manner in the buoyancy sorting scheme recently proposed by Emanuel (1991).

A simple moist convective adjustment scheme is used in the Canadian Climate Centre general circulation model (CCC GCM). This model simulates the current climate reasonably well (McFarlane et al., 1992 hereafter denoted as MBBL; Boer et al., 1992). Nevertheless, there are deficiencies in the simulated climate. One of the more pronounced of these is the one that motivated the work presented in this paper, namely that the tropical troposphere is systematically colder than the observed climatological state. Although there are several other factors that may contribute to this deficiency, the use of the moist convective adjustment to parameterize convective effects is at least partly responsible. As in other such schemes, unstable air at each layer is mixed with that in the adjacent layer above it, so that heat and moisture are transported upward while latent heat is released from the lower layer when it is found to have a relative humidity in excess of some specified threshold value. One consequence of such localized exchange is that heat and moisture are not effectively transported from the planetary boundary layer into the conditionally stable regions of the upper troposphere.

The purpose of this paper is to present a parameterization of penetrative cumulus convection that alleviates the above deficiencies in climate simulations made with the CCC GCM. This parameterization scheme utilizes some of the basic concepts set forth by Arakawa and Schubert (1974) to construct a bulk representation of the effects of an ensemble of cumulus clouds. In particular, it is assumed that these effects can be represented in terms of an ensemble of entraining updrafts with an associated evaporatively driven ensemble of convective-scale downdrafts.

A parameterization scheme based on such an ensemble concept can not be constructed in closed form without invoking a set of assumptions that enable determination of the contributions of each member of the ensemble to the total convective-scale vertical mass flux. A fundamental part of the original formulation of Arakawa

and Schubert is the quasi-equilibrium assumption which achieves this by requiring that the consumption of potential energy by the convective ensemble exactly balances the rate at which it is produced by larger scale processes. This assumption is implemented in practice by requiring that the action of the ensemble be such as to restore the work function (defined ignoring liquid water loading) for each member of the ensemble to a prescribed equilibrium value. These equilibrium values, specified as a function of the depths of the individual updrafts, are believed to be characteristic (Lord et al., 1982).

Moorthi and Suarez (1992) have shown that, in some circumstances, the standard implementation of the Arakawa-Schubert scheme as described by Lord et al. (1982) gives rise to an artificial elimination of cloud types from the ensemble. They have proposed an alternative, more economical, formulation in which relaxation to a reference state is accomplished over a period of several dynamical time steps by invoking single members of the ensemble at each of those steps and requiring that their work functions be only partially adjusted toward the specified characteristic values.

The parameterization scheme presented here was also motivated by a desire for simplicity and economy. These features are obtained by invoking two assumptions that significantly simplify implementation of the scheme. The first of these specifies the distribution of the individual drafts that are used to construct the bulk updrafts and downdrafts utilized in the scheme. It is assumed that these all have the same initial mass flux (cloud-base mass flux for updrafts, draft-top mass flux for downdrafts) and characteristic fractional entrainment rates limited to a range of values that depends on the large-scale thermodynamical structure of the atmosphere.

The second assumption is that, in the absence of other effects, cumulus convection acts to relax the atmosphere to a state that is neutrally buoyant for undiluted reversible ascent of a parcel whose initial equivalent potential temperature is equal to the large-scale mean value in the sub-cloud layer (assumed to be contained within the planetary boundary layer). A quasi-equilibrium can be established when production of convective available energy by other processes balances consumption of this quantity by moist convection.

In this paper the mathematical formulation of the new convective parameterization is presented and some features of its response to larger scale forcing conditions are illustrated by presentation of results from a simple idealized column model in which convective instability is generated and maintained by imposing a surface energy flux in association with idealized radiative cooling and large-scale ascent/descent profiles. The rest of the paper is devoted to illustration and discussion of the effects of the new convection scheme on simulations of the general circulation made with the Canadian Climate Centre GCM.

2 Convective effects on large-scale temperature and moisture fields

Cumulus convection affects the large-scale temperature and moisture fields through subgrid-scale transport and condensation. As indicated in the introductory remarks,

it is assumed here that these processes can be parameterized in terms of a quasi-steady ensemble of updrafts and downdrafts which, in accordance with the well known representation of Arakawa and Schubert (1974), gives the following formulation for the effects of cumulus convection on the larger scale temperature and moisture fields:

$$C_p\left(\frac{\partial T}{\partial t}\right)_{cu} = -\frac{1}{\rho}\frac{\partial}{\partial z}(M_u S_u + M_d S_d - M_c S) + L(c - \epsilon) \tag{1a}$$

$$\left(\frac{\partial q}{\partial t}\right)_{cu} = -\frac{1}{\rho}\frac{\partial}{\partial z}(M_u q_u + M_d q_d - M_c q) + \epsilon - c \tag{1b}$$

where the net vertical mass flux within the convective region, M_c, is made up of upward (M_u) and downward (M_d) components. Here, c and ϵ are respectively the large-scale mean rates of condensation and of evaporation; q, q_u and q_d are respectively the large-scale, and the convective scale updraft and downdraft components of the specific humidity field; and S, S_u, S_d are respectively the corresponding values of dry static energy (defined in the usual way as $S_{u,d} = C_p T_{u,d} + gz$).

In cumulus convection, high moist static energy air is transported out of the sub-cloud layer in updrafts and lower moist static energy air is imported into this layer by downdrafts. In the absence of evaporation of precipitation below cloud base, these processes give rise to temperature and moisture tendencies in the sub-cloud layer that are represented as

$$C_p\left(\rho\frac{\partial T}{\partial t}\right)_m = \frac{1}{\Delta z_b}(M_b[S(z_b) - S_u(z_b)] + M_d(z_b)[S(z_b) - S_d(z_b)]) \tag{2a}$$

$$\left(\rho\frac{\partial q}{\partial t}\right)_m = \frac{1}{\Delta z_b}(M_b[q(z_b) - q_u(z_b)] + M_d(z_b)[q(z_b) - q_d(z_b)]) \tag{2b}$$

where Δz_b is the depth of the subcloud layer, quantities with subscript m are vertical mean values for the subcloud layer, z_b is the height of the cloud base and M_b is the cloud updraft mass flux at this level. The first terms on the right-hand sides of equations (2) represent the net gain or loss of heat and moisture caused by updrafts exiting from the subcloud layer, and the second terms are those caused by downdrafts detraining into the subcloud layer.

Equations (1) and (2) are derived using the assumption, common to all such parameterization schemes, that quantities characterizing the mean environment of cumulus clouds are closely approximated by the mean values for an area, typically several thousand kilometers in magnitude, that include both the relatively small one occupied by cumulus clouds and the significantly larger one surrounding them. In the following sections, no distinction is made between such large-scale mean values and those typical of the mean environment of cumulus clouds.

3 The cloud model

a *Updraft Ensemble*

The bulk mass flux and the associated cloud properties in equations (1) and (2) represent the effects of an ensemble of cumulus clouds that may exist in a larger scale circulation regime. As in Arakawa and Schubert (1974), these effects are represented in terms of an ensemble of cloud updrafts and downdrafts. Each updraft is represented as an entraining plume with a characteristic fractional entrainment rate. Detrainment is confined to a thin layer near the plume top where the mass carried upward is expelled into the environment. The air detrained from updrafts is assumed to be saturated and have the same temperature as the environmental air. In the absence of liquid water, this air would be nearly neutral or slightly positively buoyant with respect to the local environmental air. However, since the detrained cloudy air may also contain liquid water, it may in fact be slightly negatively buoyant with respect to environmental air, or a mixture of cloudy and environmental air may in fact be slightly negatively buoyant.

This simple updraft formulation has been used extensively in observational studies of the coupling between convective systems and the larger-scale flow and thermodynamic fields. The pioneering study of Ogura and Cho (1973) showed that in the tropics, a bimodal distribution of updrafts, comprised of deep and shallow populations, is typically needed to account for the observed large-scale response to moist convection. This finding has been confirmed by later studies although it has also been found (Johnson, 1976) that allowing for convective and meso-scale downdrafts reduces somewhat the requirement for a shallow updraft population. Moreover Johnson (1976, 1980) presents evidence indicating an out-of-phase relationship between maxima in deep and shallow convective activity when the effects of convective-scale downdrafts are taken into account.

While fewer studies have been done for extra-tropical systems, the available literature suggests that they may differ somewhat from tropical ones. For example, the studies of Lewis (1975) and Zhang and McFarlane (1991) suggest that CAPE values are often larger and shallow convection is less common.

In constructing the parameterization scheme outlined below, we have chosen to focus attention on representing the effects of deep convective clouds. In the tropics, the deep convective cloud population, if represented in terms of the simple one-dimensional entraining plume updraft model, can be regarded as being comprised of those plumes which penetrate through the conditionally unstable region which typically extends up to the middle of the troposphere. A characteristics feature of this region is that the large-scale mean ambient and saturated moist static energies (h, h^*) decrease with height. Thus we assume that the top of the shallowest of the convective updrafts is no lower than the minimum in h^*.

Mainly for the sake of simplicity, we assume that the updraft population is comprised of a set of plumes that have a common value for the cloud-base mass flux. Although the studies of Ogura and Cho (1973) and Yanai et al. (1976) suggest that there may be a bias in favor of the deeper clouds, they do support the contention that there is a reasonably broad distribution of deep updrafts. The study of Johnson

(1980) suggests a significant variation in the deep cloud population throughout easterly waves that were commonly observed in the GATE region. In the trough region of the composite wave, where deep convective activity is most pronounced, detrainment occurs over a broad region from just above the level of minimum h^* to the top of the convective layer, suggesting a relatively broad spectrum of deep clouds. Thus the assumption of a uniform distribution of deep updrafts is not inconsistent with many of the observational results. It also provides useful analytical simplifications which enable us to construct a simple bulk cloud model based on the updraft ensemble concept. In particular, the ensemble cloud updraft mass flux has a simple analytical form:

$$M_u = M_b \int_0^{\lambda_D} \frac{1}{\lambda_0} e^{\lambda(z-z_b)} d\lambda = \left(\frac{M_b}{\lambda_0(z-z_b)}\right)(\exp(\lambda_D(z)(z-z_b)) - 1) \quad (3)$$

where M_b is the ensemble cloud base updraft mass flux. Interpreting this as an ensemble mass flux allows us to identify $\lambda_D(z)$ as the fractional entrainment rate of the updraft plume that detrains at height z, while λ_0 is the maximum entrainment rate allowed. The mass flux at the base of the convective layer is $(M_b d\lambda/\lambda_0)$ for that plume with fractional entrainment rate in the interval $(\lambda, \lambda + d\lambda)$.

The quantity λ_D is defined by the requirement that the temperature of the plume that detrains at height z is equal to the environment value, which is ensured by requiring that

$$h_b - h^* = \lambda_D \int_{z_b}^{z} [h_b - h(z')]\exp[\lambda_D(z' - z)]dz' \quad (4)$$

where h^* is the moist static energy for a saturated state having the environmental temperature and pressure.

In equation (4) the moist static energy profile, $h(z)$, is presumed to be known. As this equation is non-linear in λ_D, it must be solved by an appropriate numerical method. In practice, a Newton-Raphson procedure generally converges rapidly with a reasonable first guess. We have also found that a quite accurate non-iterative approximate solution can, in most circumstances, be obtained using the reversion of series procedure outlined in the Appendix.

For a typical conditionally unstable atmospheric column, $\lambda_D(z)$ has a maximum in the lower troposphere and decreases with height. The maximum entrainment rate λ_0, which is associated with the shallowest plume of the ensemble, must be set. This is done by making use of the fact that h^* typically has a minimum in the middle troposphere in a conditionally unstable atmosphere. The ensemble is limited to updrafts that detrain at or above the height of minimum h^*. Thus if z_0 is this height, $\lambda_0 = \lambda_D(z_0)$ is the maximum entrainment rate in the cloud ensemble. This choice insures that detrainment is confined to the conditionally stable region of the atmospheric column.

In practice, $\lambda_D(z)$ is evaluated numerically for each layer in the model by pro-

ceeding downward from the top of the convective region in the upper troposphere and in typical cases, it is single-valued above z_0 and decreases with height. However, if h^* has secondary minima between the top of the convective region and z_0, $\lambda_D(z)$ will not vary monotonically with height. In such cases, $\lambda_D(z)$ is set to the larger of the values obtained for the ambient layer and the layer directly above it.

Detrainment is confined to regions where $\lambda_D(z)$ decreases with height so that the total detrainment $D_u(z)$ is zero below z_0 and

$$D_u(z) = -\frac{M_b}{\lambda_0}\frac{\partial \lambda_D}{\partial z}\exp(\lambda_D(z)(z - z_b)) \tag{5a}$$

above z_0. The corresponding total entrainment rate is given by

$$E_u = \frac{M_b}{\lambda_0}\int_0^{\lambda_D} \lambda e^{\lambda(z-z_b)} d\lambda = \frac{\partial M_u}{\partial z} - D_u. \tag{5b}$$

It is assumed that the air that detrains from the convective ensemble is saturated at the environmental temperature and pressure. All condensation occurs within updrafts (i.e., $c = C_u$). Condensed water detrained from updrafts evaporates locally into the environment. With these assumptions, the equations governing the budgets of ensemble mean dry static energy S_u, water vapor mixing ratio q_u and cloud water content l for cloud updrafts are

$$\frac{\partial}{\partial z}(M_u S_u) = (E_u - D_u)S + LC_u \tag{6a}$$

$$\frac{\partial}{\partial z}(M_u q_u) = E_u q - D_u q^* - C_u \tag{6b}$$

$$\frac{\partial}{\partial z}(M_u l) = -D_u l_d + C_u - R_r \tag{6c}$$

where C_u and R_r are respectively the net condensation and conversion from cloud liquid water to rainwater in the updrafts and l_d is the liquid water content of detrained cloudy air, for simplicity taken here to be identical to the ensemble mean cloud water, l.

Conversion of cloud water to rainwater is represented using the empirical formulation discussed by Lord (1982). In this formulation, precipitation production is taken to be proportional to the vertical flux of cloud water in the updraft as

$$R_r = C_0 M_u l \tag{7}$$

where $C_0 = 2 \times 10^{-3}$ m^{-1}. Lord (1982) notes that this simple representation of precipitation production has been found to give good agreement with observed liquid water contents in observational studies of tropical convective systems.

While the focus of our parameterization is on deep clouds, there are circum-

stances in which the cumulus cloud population is predominantly shallow. This is typically true in the trade-wind convective regime where large-scale subsidence acts to suppress deep convection. The shallow cloud population which develops in this regime acts predominantly to moisten and cool the upper part of the convective layer and to warm and dry the lower part. Precipitation rates are relatively small so that the net convective heating is also small. In an overall sense, cumulus clouds act predominantly to re-distribute heat and moisture within the convective layer. Studies of the heat and moisture budgets of the Trade Wind boundary layer (e.g. Betts, 1975, 1982; Cho, 1977) raise doubts about the adequacy of the simple one-dimensional steady-state updraft model as a means of representing the effects of cumulus clouds in this regime. Cloud life-cycle effects, cloud top entrainment, and non-penetrative downdrafts may all be important. However, the broad features of cumulus cloud effects can be captured at least qualitatively by limiting the production of precipitation in shallow updrafts. Cooling and moistening in the upper part of the cloud layer is then represented as *in-situ* evaporation of detrained cloud water while heating and drying in the lower part is associated with compensating subsidence. In reality of course, most of the evaporation probably occurs in shallow downdrafts originating near cloud tops.

The practice of inhibiting rain water production within a region directly above cloud base is also used in other parameterization schemes (Tiedtke, 1989; Emanuel, 1991; Slingo et al., 1994) but the depth of this region is usually specified and invariant with location. Here we suppress conversion of cloud water to rain water below the freezing level so that shallow convection does not generate precipitation. In practice, the pressure at the freezing level is usually near 600 mb in the tropics and the sub-cloud layer is typically of the order of 500 m deep so that the depth of the region in which precipitation production is inhibited is usually in the range of 3 to 4 km in the tropics. These values are comparable to those specified in other schemes. However, we do recognize that this admittedly *ad-hoc* limitation of precipitation production to clouds which extend above the freezing level may have shortcomings. It does not account for circumstances (e.g. over the tropical oceans) where weak environmental winds and high liquid water contents may promote substantial precipitation from shallower clouds. Some authors (e.g. Slingo et al., 1994) attempt to account for this in a simple and practical way by assigning fixed but different depths for non-precipitating cumulus clouds over land and ocean surfaces.

b *Downdraft Ensemble*

Downdrafts have been found important in the interaction between cumulus convection and larger-scale processes. Indeed, the marked cooling and drying of the sub-cloud layer that often follows organized convection in both the tropics and the mid-latitudes (e.g. Frank and McBride, 1989; Zhang and McFarlane, 1991) is likely the result of detrainment of low energy air imported from mid-tropospheric levels by downdrafts.

In this study, downdrafts are assumed to exist when there is precipitation production in the updraft ensemble. The downdrafts start at or below the bottom of the updraft detrainment layer, which as indicated above is also the layer in which the minimum in h^* occurs and penetrates down to the sub-cloud layer. Knupp (1987) provides some observational evidence to support such a choice for the level at which penetrative downdrafts are established. There are also studies (Betts, 1976) which lend some support to the idea that penetrative downdrafts originate closer to the base of the convective layer. In the present study, the downdraft initiation level is chosen to be coincident with the minimum of h if lower than the base of the detrainment layer. This assumption is used by Grell et al. (1991) in a version of the Arakawa-Schubert scheme which includes saturated downdrafts. Their study suggests, on the basis of semi-prognostic tests, that initiation of saturated downdrafts at this level, so that they can transport lower-energy air more efficiently to the sub-cloud layer, may be preferable to initiating them higher up in the convective region. Detrainment of downdrafts is confined to the subcloud layer. As for updrafts, it is assumed that the bulk effect of downdrafts can be represented in terms of an ensemble of plumes that have the same mass flux at the top of the downdraft region. The initial downward mass flux for this ensemble is taken to be proportional to the cloud base mass flux for the updraft ensemble. With these assumptions, the ensemble downdraft mass flux is given by

$$M_d = \frac{-\alpha M_b}{\lambda_m(z_D - z)}\{\exp(\lambda_m(z_D - z)) - 1\} \tag{8}$$

where λ_m is the maximum downdraft entrainment rate.

The proportionality factor, α, is chosen so as to ensure that the strength of the downdraft ensemble is constrained both by the availability of precipitation and by the requirement that the net mass flux at cloud base be positive (i.e. upward). The total precipitation, produced in updrafts between cloud base (z_b) and the top of the convective layer (z_T) is given by

$$PCP = \int_{z_b}^{z_T} R_r dz. \tag{9}$$

It is assumed that the downdrafts are maintained in a saturated state by evaporation of rain water. The evaporation, per unit of α, in downdrafts is given by

$$EVP = \left(\frac{1}{\alpha}\right)\int_{z_b}^{z_D}\left(\left(\frac{\partial}{\partial z} M_d q_d - E_d q\right) dz\right). \tag{10}$$

The proportionality factor is chosen to be of the form

$$\alpha = \mu\left[\frac{PCP}{PCP + EVP}\right]. \tag{11}$$

This form for α ensures that the downdraft mass flux vanishes in the absence of precipitation. It also ensures that evaporation in the downdraft can not exceed a fraction μ of the precipitation. We have also chosen to impose the constraint that the net mass flux at cloud base must be positive. This constraint is ensured by requiring that

$$\mu \leq \lambda_m(z_D - z_b)/(\exp[\lambda_m(z_D - z_b)] - 1). \tag{12}$$

For most of the work presented below, μ has the fixed value of 0.2 and, consistent with the idea that downdrafts have substantially higher entrainment rates than the corresponding updrafts, $\lambda_m = 2\lambda_0$ (as in Zhang and Cho, 1991) but is also constrained to be no larger than

$$\lambda_{\max} = 2/(z_D - z_b). \tag{13}$$

This constraint on λ_m ensures that the magnitude of the downdraft mass flux at cloud base is no larger than 65% of the corresponding updraft mass flux. As demonstrated below, single column tests show that the factor $PCP/(PCP+EVP)$ in equation (11) is in general sufficiently small to ensure that the actual magnitude of the downdraft mass flux at cloud base is substantially less than that of the associated updraft.

Johnson (1978) finds considerable variation in the optimal value of α within tropical waves. In the southern portion of the composite wave that he analyses, the values of this quantity are as large as 0.67 and the corresponding ensemble downdraft mass flux at cloud base has a magnitude which is about one half that of the corresponding updraft mass flux. In contrast, values of α in the central portion of the wave do not exceed 0.5.

Some interesting responses were found in single-column model tests when μ is given by the equality condition in equation (12). As illustrated below, the typical magnitude of the downdraft mass flux at cloud base for this choice is close to one-half that of the updraft mass flux, typical of the larger values shown in Johnson's (1978) paper. In some circumstances, this "strong" downdraft formulation gives rise to a temporally variable convective regime in which both deep and shallow updrafts are present. Selected results from these tests are presented in section 5 below.

4 Closure condition

As discussed in section 1 above, the closure condition used here is based on the assumption that cumulus clouds consume convective available potential energy at a specified rate. We define this quantity as

$$A = g \int_{IL}^{EL} \frac{(\Theta_{vp} - \Theta_v)}{\Theta_v}\, dz \tag{14}$$

where $\Theta_{vp} = \Theta_p(1 + 1.608q_p - q_m)$ is the virtual potential temperature of undiluted air parcels following a reversible moist adiabat; and $\Theta_v = \Theta(1 + 0.608q)$ is the

large-scale virtual potential temperature. Subscript p is for parcel properties and IL and EL are, respectively, the parcel-originating level and the equilibrium level in the upper troposphere where air parcels become non-buoyant, and q_m is the water vapor mixing ratio at IL.

It is shown in section 2 that the large-scale temperature and moisture changes in both the cloud layer and sub-cloud layer are linearly proportional to the cloud base updraft mass flux M_b. Therefore, the CAPE change due to convection can be symbolically written as:

$$\left(\frac{\partial A}{\partial t}\right)_c = -M_b F \tag{15}$$

where F is the CAPE consumption rate per unit cloud base updraft mass flux. This quantity, which is required to be positive for cumulus convection to exist, is evaluated by formally differentiating the integrand in (14) with respect to t and substituting from equations (1) and (2), evaluated for unit mass flux using the updraft/downdraft properties determined as discussed in the foregoing section. The contributions associated with variations of Θ_{vp} are due to the effects of convection on the sub-cloud layer as expressed in equations (2) while those due to variation of Θ_v are due to the large-scale effects of moist convection in the cloud layer as expressed in equation (1).

The closure condition in this study is that CAPE is consumed at an exponential rate by cumulus convection with characteristic time scale τ. This assumption implies that

$$M_b = \frac{A}{\tau F}. \tag{16}$$

Sensitivity to the choice of the time scale is discussed in the following section in the context of a simple single-column model.

5 Results from single column tests

This section is devoted to presentation of results from tests of the convective scheme using a simple single-column model in which convective available energy is generated by the combined action of surface fluxes of heat and moisture, radiative cooling, and large-scale ascent. These processes are specified in simple idealized ways. Pressure is used as a vertical coordinate with equally spaced layers, 50 mb in depth, between the 1000 and 50 mb levels. The large-scale variables (T and q) are specified at the mid-layer pressure levels 975, 925, ..., 75 mb. The cloud properties M_u, M_d, M_c, S_u, S_d, q_u, q_d, l are at the levels of the layer interfaces and the rest of the cloud properties (D_u, E_u, E_d, C_u) are at the mid-layer levels.

A time step of 20 minutes is used for all of the model experiments in this study. Initial values of the large-scale variables (T, q) are specified using a mean sounding from the GATE data.

TABLE 1. Summary of column model experiments.

Exp. No.	τ (hours)	Downdraft Strength (μ)	Max. Top (Mb)	Large-scale vertical vel.	CAPE(J/Kg) Char.	max.	mean	min.
1	2	0.2	200	No	Steady		800	
2	4	0.2	200	No	Steady		1400	
3	6	0.2	200	No	Steady		1800	
4	2	Str.	150	No	Fluct.	1000	650	400
5	2	Str.	150	Periodic	Periodic and Fluct.	1100		100

a *"Convective-Radiative" Equilibrium*

In the "convective-radiative" equilibrium test, the atmosphere is forced by a specified cooling rate in the troposphere ("radiative cooling") and sensible and latent heat fluxes at the surface. Dry adjustment is activated when the atmosphere is statically unstable. Large-scale condensation occurs when the atmosphere reaches saturation. The radiative cooling rate is constant from 150 mb to the surface, with a magnitude of $2 \times 10^{-5}(°C/s)$, and decreases linearly to zero at and above the 100 mb level.

Sensible and latent heat fluxes at the surface (assumed to have a fixed pressure of 1000 mb) are specified using the following bulk aerodynamic formulae:

$$F_s = C_D V(\Theta_s - \Theta_1)\rho_s \tag{17a}$$

$$F_q = C_D V(q_s - q_1)\rho_s \tag{17b}$$

where $C_D = 2 \times 10^{-3}$ is the drag coefficient, V is a typical surface wind speed, Θ_s and Θ_1 are respectively the potential temperature at the surface and the lowest model layer, q_1 and q_s are respectively the lowest model-level water vapor mixing ratio and the surface saturation value. Here we use $\Theta_s = 300$ K, $V = 5$ m s^{-1}.

Numerous tests were made with this simple column model. Selected results from these tests are summarized in Table 1 and some of the experiments are discussed more fully below. The results of the first three experiments, summarized in Table 1, reveal that a nearly steady equilibrium state, in which there is a finite amount of CAPE, is reached when the simple radiative convective configuration of the model is used. The time required to achieve equilibrium and the magnitude of the final value of CAPE both depend on the choice of the adjustment time, τ. A consequence of the proportionality between the equilibrium value of CAPE and τ is that the cloud-base mass flux and the convective precipitation rate are almost independent of τ at equilibrium.

Fig. 1 displays the vertical profiles of the cloud mass flux, entrainment and detrainment averaged over the last 500 hours of the time integration for the first

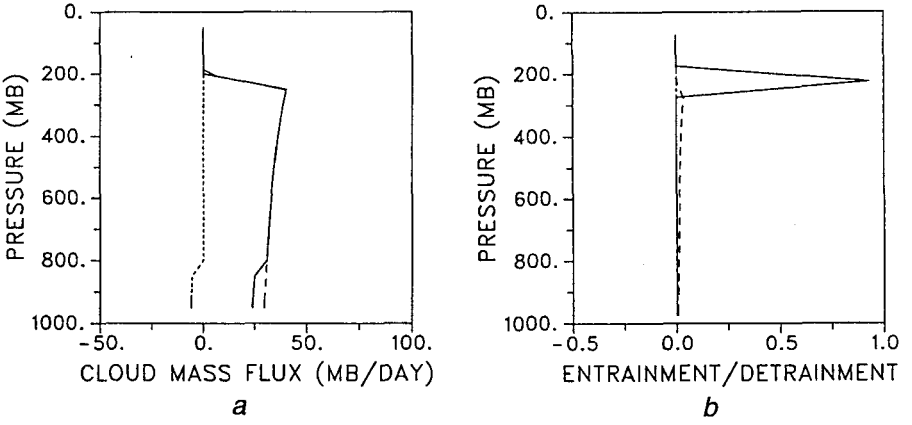

Fig. 1 Vertical profiles of *a*) net cloud mass flux (solid line), updraft mass flux (dotted line) and downdraft mass flux (dashed line), units: mb day; *b*) updraft mass detrainment (solid line), updraft mass entrainment (dashed line) and downdraft mass entrainment (dotted line), units: 10^{-5} s^{-1}.

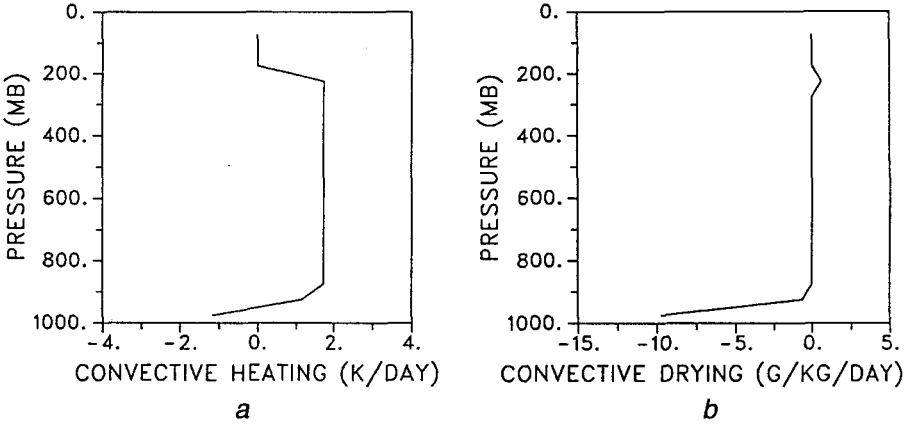

Fig. 2 Vertical profiles of *a*) convective heating (units: °K/day) and *b*) convective drying (units: g/kg/day).

experiment in Table 1. The convective heating and drying profiles are shown in Fig. 2 and the corresponding profiles of h, h^*, specific humidity, and dry static energy (normalized by C_p) are shown in Fig. 3. The weak shallow downdraft, relatively weak entrainment and strong detrainment in a narrow region at the top of the convective layer are related to the vertical structure of h and h^*. The marked difference between the initial and equilibrium structures of these quantities, especially with regard to the moist static energy, is a consequence of a pronounced drying and a moderate warming in the convective layer. Since surface evaporation is the only

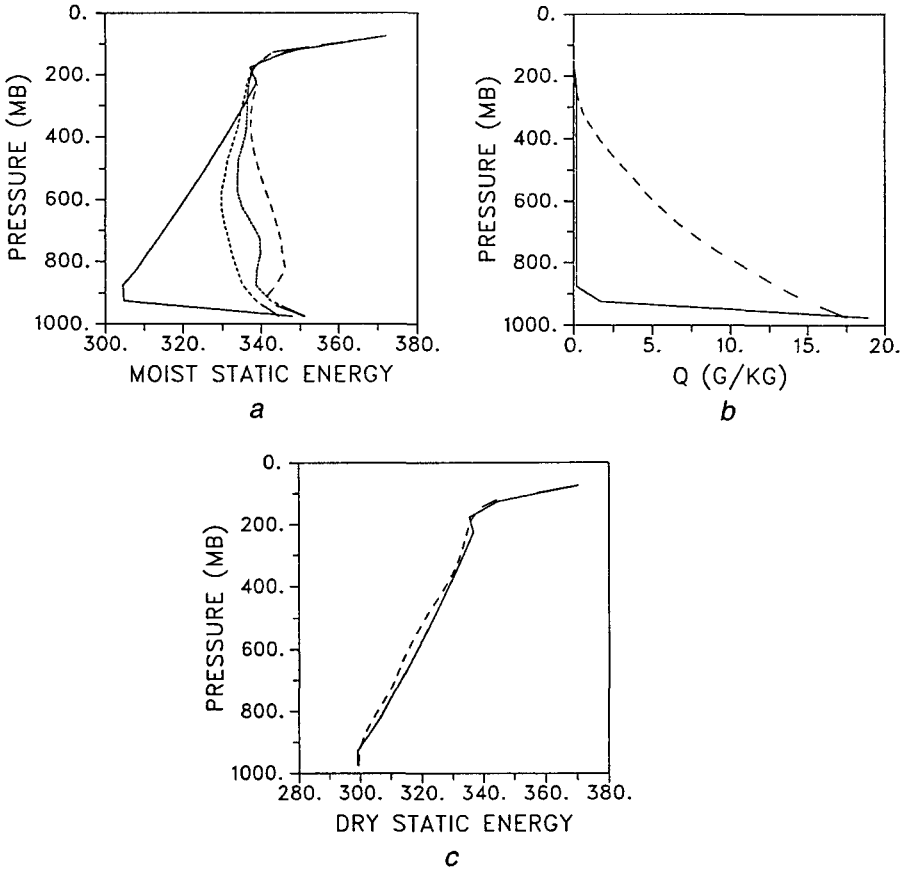

Fig. 3 Vertical profiles of *a*) the moist static energy and its saturation value; the solid line and the long dashed line are the averaged actual and saturation moist static energy, the short-dashed and the dotted lines are those at the initial time, respectively, units: J/kg; *b*) averaged water vapor mixing ratio (solid line) and initial state (dashed line), units: g/kg; *c*) averaged dry static energy (normalized by the heat capacity of the air C_p = 1004.6 J/kg/K) (solid line) and initial state (dashed line), units: °K.

imposed moisture source in this experiment, the equilibrium state is one in which there is no net moisture tendency in the convective layer. The humidity structure required to ensure this is one in which the vertical gradient of q vanishes within the convective layer. Within the detrainment layer (which is confined to a single model layer), the environment is saturated and detrainment of cloud water is balanced by large-scale condensation. Thus the specific humidity is constant everywhere within the convective layer and equal to the saturation value at the mid-point of the detrainment layer.

The shallowness of downdrafts in the experiment discussed above is a direct

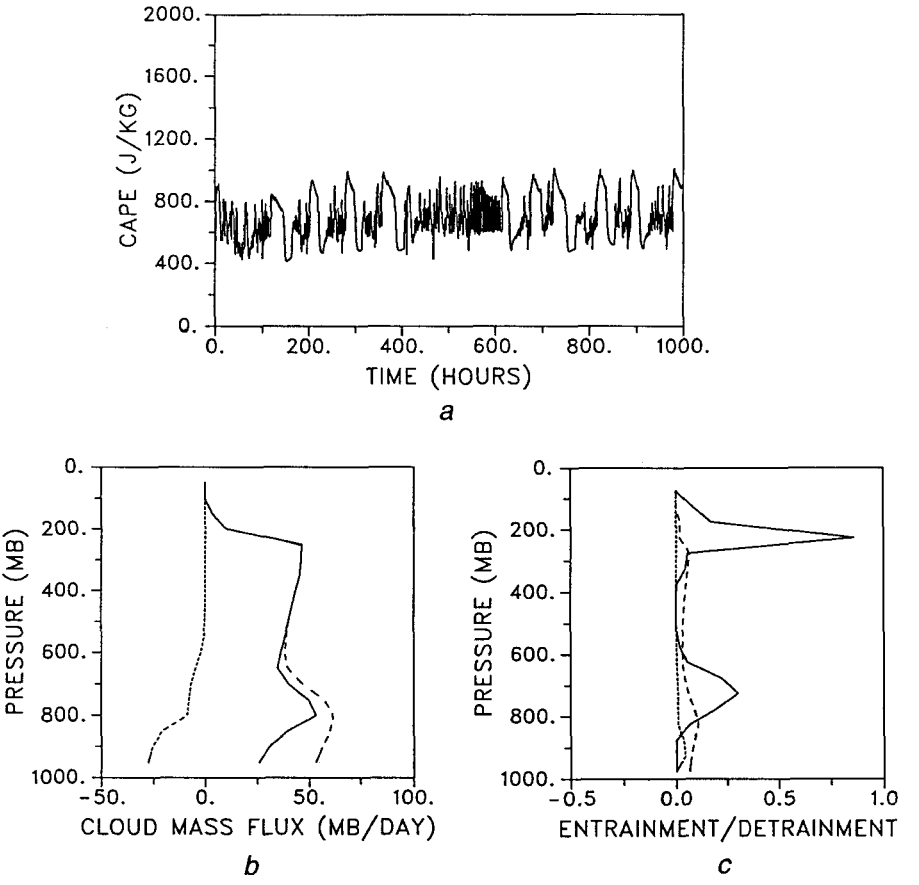

Fig. 4 *a*) Time evolution of CAPE for the stronger downdraft experiment. *b*) and *c*) are the same as Figs. 1*a* and 1*b* except with stronger downdrafts.

consequence of the assumption that they start from the level of minimum h. It is noteworthy that, despite being rather shallow and weak, they do account for most of the convective cooling and drying in the sub-cloud layer, as shown in Fig. 2.

The quasi-steady equilibrium illustrated in Fig. 2 is associated exclusively with deep convective clouds. Although we have not attempted to devise a distinct parameterization for shallow cumulus clouds, we have found that using the "strong downdraft" formulation, as defined in section 4 above, results in a much less regular temporal behavior, in which shallow clouds occur spontaneously. This is illustrated in Figure 4a which shows the time evolution of CAPE for the "strong downdraft" case (exp. 4 in Table 1). The nearly steady equilibrium found in the previous experiment is replaced by one in which CAPE varies irregularly from about 400 J/kg to 1000 J/kg. The mass flux and the entrainment/detrainment profiles, averaged over the last 500 hours (Figures 4b and 4c), are distinctly different as well. The updraft

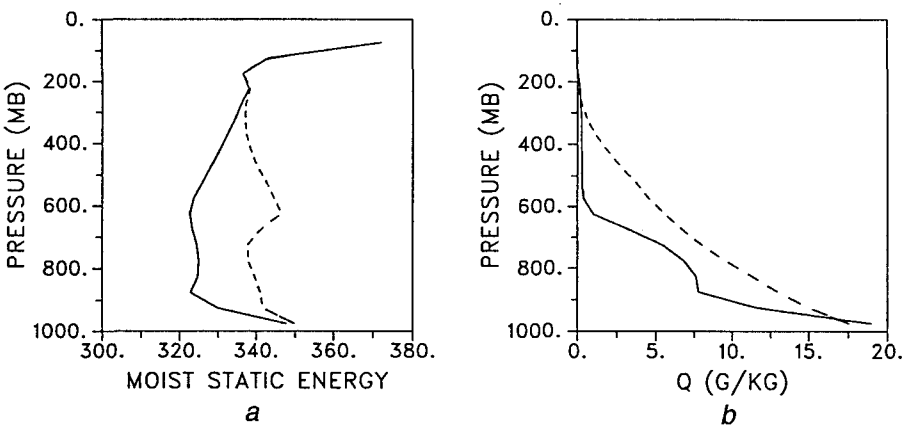

Fig. 5 Vertical profiles for the strong downdraft experiment. *a*) Moist static energy (solid line) and its saturation value (dashed line), *b*) water vapor mixing ratio (solid line) and its initial value (dashed line). Units are as in Fig. 3.

mass flux has a lower-level maximum at 800 mb and a second upper-level maximum at 200 mb, the lower one being the result of a greater abundance of shallower convection events in this experiment. This is also reflected in the mean vertical structure of the updraft detrainment which has two distinct maxima, the lower one (at 700 mb) being associated with shallower convective events. The mean downdraft is associated exclusively with the deeper convective events and is relatively stronger than in the previous experiments.

The lower half of the troposphere is moister (Fig. 5b) due to moistening by the liquid water and moist air detrained from shallow convection. The cooling associated with evaporation of detrained liquid water is reflected in the mean vertical structure of the moist static energy (Fig. 5a), which has an inversion near the top of the region occupied by shallow convection.

The results shown in the above experiments clearly demonstrate the potential importance of downdrafts in the convective stabilization process. The cooling and drying of the sub-cloud layer due to downdrafts acts to stabilize the atmosphere column. However, for the simple column model used here, this effect is relatively small for weaker downdrafts and is easily offset by surface heat and moisture fluxes and the imposed radiative cooling. It is possible in these circumstances to achieve a quasi-steady equilibrium between the convective stabilization and the forced large-scale destabilization. On the other hand, strong downdrafts provide a powerful mechanism for stabilizing the atmospheric column. When these are present, deep convection may occur intermittently because it consumes CAPE more rapidly than CAPE is built up by the large-scale processes. In the time periods between deep convective events, shallow convection develops and prevails until the convectively unstable layer becomes sufficiently deep that a deep convection episode can again occur.

The presence of both deep and shallow convection produces the double peak structure in time-averaged cloud updraft mass flux and detrainment profiles as shown in Fig. 4. In this respect, our results are qualitatively similar to those obtained by Satoh and Hayashi (1992) using a simple radiative-convective model in which cumulus convection is parameterized in terms of a bulk updraft cloud model in which the mass flux is assumed to be proportional to the amount of convective instability. They found that, for large proportionality constants (i.e. larger mass fluxes for a given amount of convective instability), the temporal evolution is irregular and is characterized by the intermittent occurrence of both shallow and deep convection. However, for a sufficiently small proportionality constant, only deep convection exists and a steady equilibrium is obtained.

b *Effects of Imposed Large-scale Vertical Motion*

It is well known that deep convection in the atmosphere is enhanced in regions of large-scale ascent and suppressed in regions of subsidence. In this section, results are presented from experiments in which, in addition to the prescribed "radiative cooling", a large-scale vertical motion profile is also imposed. This is specified in terms of the total time derivative of pressure ($\omega = dp/dt$) which is specified in the following form:

$$\omega = 4\omega_m(p_0 - p)(p - p_1)/(p_0 - p_1)^2 \tag{18}$$

where $p_0 = 1000$ mb and $p_1 = 150$ mb. The maximum vertical motion, ω_m, occurs at 575 mb.

The maximum ascent typical of mean conditions in convergence zones of the tropics is of the order of a few tens of millibars per day. Wavelike synoptic-scale disturbances in the tropics impose a fluctuating component on this mean state such that large-scale ascent is enhanced in the trough regions of the waves while vertical ascent is suppressed in the ridges. To simulate the convective response in such circumstances, we impose the following temporally periodic amplitude factor,

$$\omega_m = -75[1 + \cos(2\pi t/\tau_s)] \tag{19}$$

where the period, τ_s, of the imposed sinusoidal variation is specified to be 5 days and the units of ω_m are (mb)/(day).

In general we have found that the convective response is controlled by the imposed vertical motion even when strong downdrafts are allowed in the convection scheme. Figure 6 shows the temporal evolution of CAPE for such a case (exp. 5). The rather irregularly fluctuating character associated with strong downdrafts is strongly modulated by a periodic component of temporal variation which is the response to that in the imposed large-scale ascent profile. A similar behavior is found for convective precipitation (not shown) which has a periodic component that varies between 5 mm/day in the undisturbed sector and 18 mm/day in the dis-

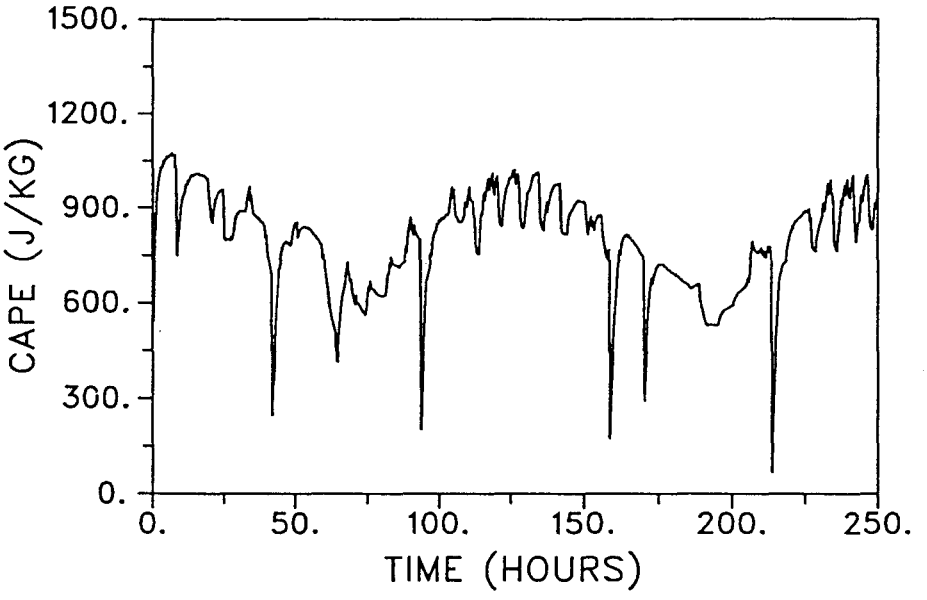

Fig. 6 Evolution of CAPE for the temporally varying large-scale ascent case.

turbed part. It also has irregular fluctuations imposed on this periodic component. The effect of these is to make the precipitation range somewhat larger (between 0 and 22 mm/day). The predominance of the periodic component of the response, evidence of a quasi-equilibrium between the imposed large-scale forcing and the convective response, is established quickly.

Other features of the quasi-equilibrium nature of the convective response to the imposed large-scale forcing are apparent in Figure 7, which depicts the ensemble mean profiles of the convective mass flux and associated updraft detrainment rate for disturbed and undisturbed periods. These profiles were obtained by separately averaging the relevant quantities for 8 periods of enhanced ascent (disturbed periods) and the associated 8 periods of reduced ascent (undisturbed periods).

The vertical structure of ensemble mean mass flux (Figure 7a) during disturbed periods is similar to that of the imposed vertical motion field, reflecting the fact that large-scale forcing during these periods is predominantly due to the imposed vertical ascent. However, during undisturbed periods, the mean vertical ascent is much weaker so that the imposed radiative cooling makes a relatively larger contribution to the large-scale forcing. The time-averaged vertical profile of the mass flux in this regime has two maxima, indicating a bi-modal character for the convection.

The detrainment profiles also clearly reflect the different characteristics of the two regimes. The double maxima present in the mean detrainment profile for the undisturbed periods indicates that in this regime the convective response consists

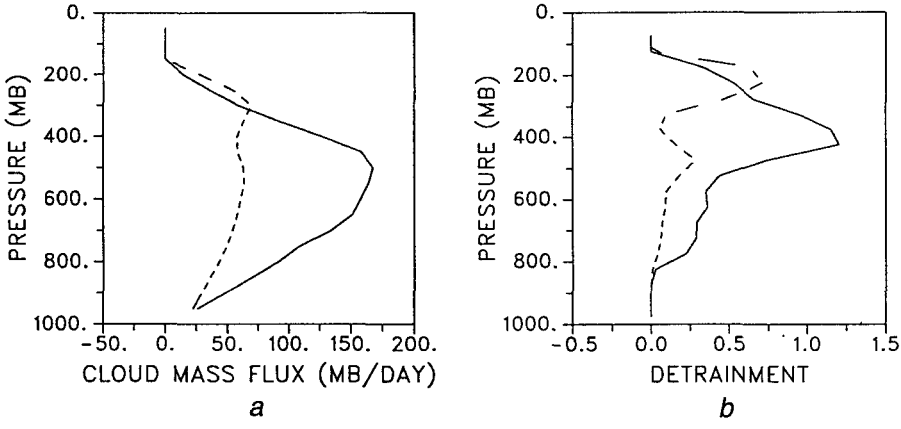

Fig. 7 Vertical profiles of net mass flux and detrainment for the large-scale ascent case. Solid, disturbed cases, dashed, undisturbed periods.

of contributions from both deep and shallow elements. In contrast, the broad single maximum of mean detrainment that is found in the upper troposphere during the disturbed periods is characteristically associated with a predominance of deep convection. The presence of significantly non-zero detrainment values throughout the region between the 500 and 800 mb levels confirms, however, that shallower convective elements are also sufficiently abundant to make a significant contribution. The broader spectrum of convective elements excited during disturbed periods is the convective response needed to offset the enhanced destabilization in the middle part of the troposphere associated with the imposed large-scale vertical motion field.

The over-all behavior of the convective activity in this simple simulation of the response to tropical wave forcing is broadly similar to that shown by Johnson (1980) although unlike his scheme, ours does not include mesoscale downdrafts. Although shallower clouds are present in our simulation, the shallow cloud population differs from that found by Johnson (1980). In his results, shallow clouds are predominant in the undisturbed portion of the wave and detrain mainly in the lower troposphere. This type of response is suppressed in our simulation largely as a result of our assumption that no detrainment occurs in the region below the minimum in h^*.

We have also carried out an experiment designed to simulate the effects of large-scale subsidence in suppressing deep convection. In this case, only non-precipitating shallow convection occurs. The effects of convection are entirely confined to the region below the 700 mb level. The heating and drying profiles (not shown) for this case show that cooling and moistening occur in the upper part of the convective layer in association with detrainment of cloud water while warming and drying occur in the lower part. These processes maintain a well defined convective boundary layer capped by a sharp inversion, qualitatively similar to what is found in the trade-wind regime.

This is of course an expected result which is consistent with those demonstrated in other studies (e.g. Tiedtke, 1989; Gregory and Rowntree, 1990). We also find, as did those authors, a tendency of the scheme to produce near-saturated conditions at the base of the inversion, possibly indicative of insufficient vertical mixing at the top of the convective layer. We have not, however, followed their lead in attempting to correct this in the simple column model by forcing the scheme to over-shoot into the inversion. Gregory and Rowntree (1990) note that such split final detrainment schemes can, with quite reasonable assumptions, lead to excessive moistening and cooling in the inversion layer. Moreover, the simple column model used here does not include the vertical mixing from background diffusion and radiative feed-back processes that are part of the full GCM.

c *Moist Convective Adjustment*

The results of the simple column model experiments discussed in the foregoing sections have illustrated the effect of the penetrative cumulus convection scheme in a variety of situations. It is natural to ask how different these results are from those that are obtained with the simple column model using the moist convective adjustment scheme currently employed in the CCC GCM (MBBL). Fig. 8 shows the thermodynamic structure averaged over the last 500 hours for the "convective-radiative" equilibrium obtained with the simple column model using this moist convective adjustment scheme. The moist static energy profiles (Fig. 8a) indicate that the equilibrium atmospheric state is conditionally unstable throughout the troposphere. The minimum of the moist static energy is located in the upper troposphere near the 175 mb level whereas in the corresponding deep convection simulation it is located below the 800 mb level.

In contrast to the penetrative convection scheme, the convective adjustment scheme is local in nature. It checks the stability of an air column, layer by layer, starting from the lowest pair of layers. Air is exchanged between adjacent layers where the lapse rate at the interface between them exceeds an imposed threshold value. This threshold value is chosen to be a linear combination of the wet and dry adiabatic values with weighting such that the wet adiabatic value is used when the relative humidity of the lower layer is 100%. Any supersaturation which remains after, or results from, this exchange process is condensed and precipitated. Clearly this process is much less efficient than the penetrative convective parameterization at transporting moist static energy from the lower levels to the upper troposphere. Comparison between the moist static energy and its saturation value indicates that the atmosphere is very close to saturation whereas the air in the deep convection runs is far from saturated.

Fig. 8b displays the time-averaged moisture structure in comparison with the initial state. The averaged state is moister below the 500 mb level and drier above. This is qualitatively different from what is found in the penetrative convection runs, where the air is much drier in the middle and lower troposphere (except the subcloud layer) and moister in the upper troposphere. The dry static energy profiles

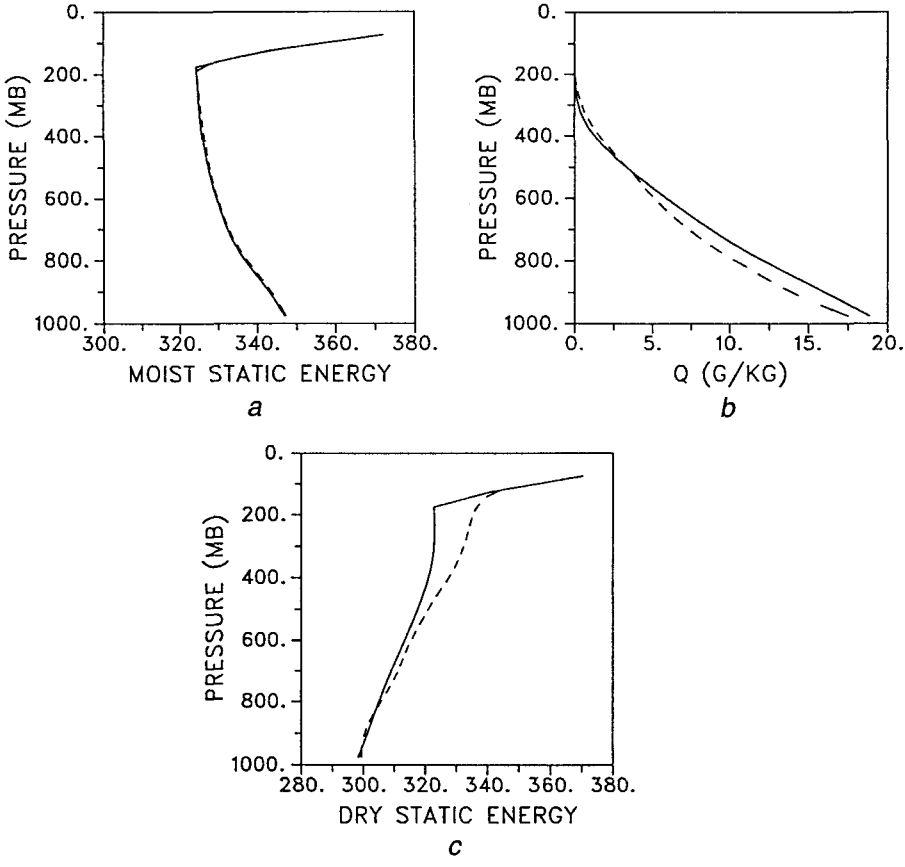

Fig. 8 Vertical profiles of *a*) moist static energy (solid line) and its saturation value (dashed line) *b*) water vapor mixing ratio (solid line) and its initial value (dashed line) and *c*) dry static energy (solid line) and its initial value (dashed line) for the moist convective adjustment experiment.

(Fig. 8c) show that the averaged atmosphere is less dry-statically stable and colder than the initial state in the upper troposphere. It is slightly warmer just above the subcloud layer. This is again in qualitative contrast to the results for the deep convection runs where the air is warmer almost everywhere, especially in the upper half of the troposphere. Due to the inefficiency in the vertical transport through convective adjustment, the moisture provided through surface evaporation tends to accumulate in the lower troposphere.

6 Effect on GCM climate simulations

The new cumulus parameterization has also been tested in the second generation version of the CCC GCM (McFarlane et al., 1992, hereafter referred to as MB-BL). This version of the GCM also contains a simple thermodynamic oceanic

mixed-layer module coupled to a thermodynamic sea-ice module. The internal heat transports in the oceanic mixed layer and the vertical heat transport at the lower boundary of the sea ice are specified as outlined in MBBL. These specified internal heat transports are retained in unmodified form in the version of the GCM which contains the new cumulus parameterization. This allows direct comparison to the multi-year climate simulation (hereafter referred to as the CONTROL simulation) that has been documented by MBBL.

For the experiment in which the cumulus parameterization is used for the climate simulation, the moist convective adjustment scheme in the operational version of the CCC GCM is modified so that it acts only to remove dry static instabilities. Apart from these modifications, the version of the GCM used is as described by MBBL.

The climate simulation using the penetrative convection scheme was initiated from a May 1 restart file of the multi-year simulation made with this standard version of the GCM. The experimental simulation (hereinafter referred to as the CONV simulation) was terminated at the end of February of the third simulated year. A significant amount of "climate drift" is apparent in the last two years of the CONV simulation. Reasons for this are discussed below. The results shown in the following sub-sections are ensemble means for the December–February and June–August periods unless otherwise indicated.

a *Zonal Mean Temperature and Moisture Fields*

The CONTROL climate simulation has a cold bias throughout the tropical troposphere in all seasons. Implementing the penetrative cumulus parameterization removes this bias and, in fact, replaces it with a warm bias in the upper troposphere. This is illustrated in Figure 9 which shows the zonally averaged differences between simulated temperature fields and 9-year ensemble means of objectively analysed fields produced at the ECMWF.

Figure 10, which depicts the corresponding specific humidity anomalies, shows that implementation of the penetrative convection scheme also results in a drier lower troposphere in the tropics. This effect is quite consistent with the results of the column tests discussed above. However, in this case it enhances the dry anomaly which is already present in the CONTROL simulation. In part, this feature may be associated with an inadequate representation of the effects of shallow convection. Results of other shorter simulations (not shown) also indicate that this dry anomaly is reduced, but not removed, by implementing the "strong downdrafts" version of the convection scheme.

Other experiments also reveal, not surprisingly, that the vertical structure of the humidity field in the lower troposphere is sensitive to vertical resolution and the treatment of vertical transfer of moisture due to turbulent mixing in the boundary layer. The zonally averaged relative humidity structure for both simulations shows a tendency for trapping of moisture near the surface, suggesting that in both experiments there may be insufficient vertical transfer of moisture due to a combination of boundary-layer processes and shallow cumulus convection.

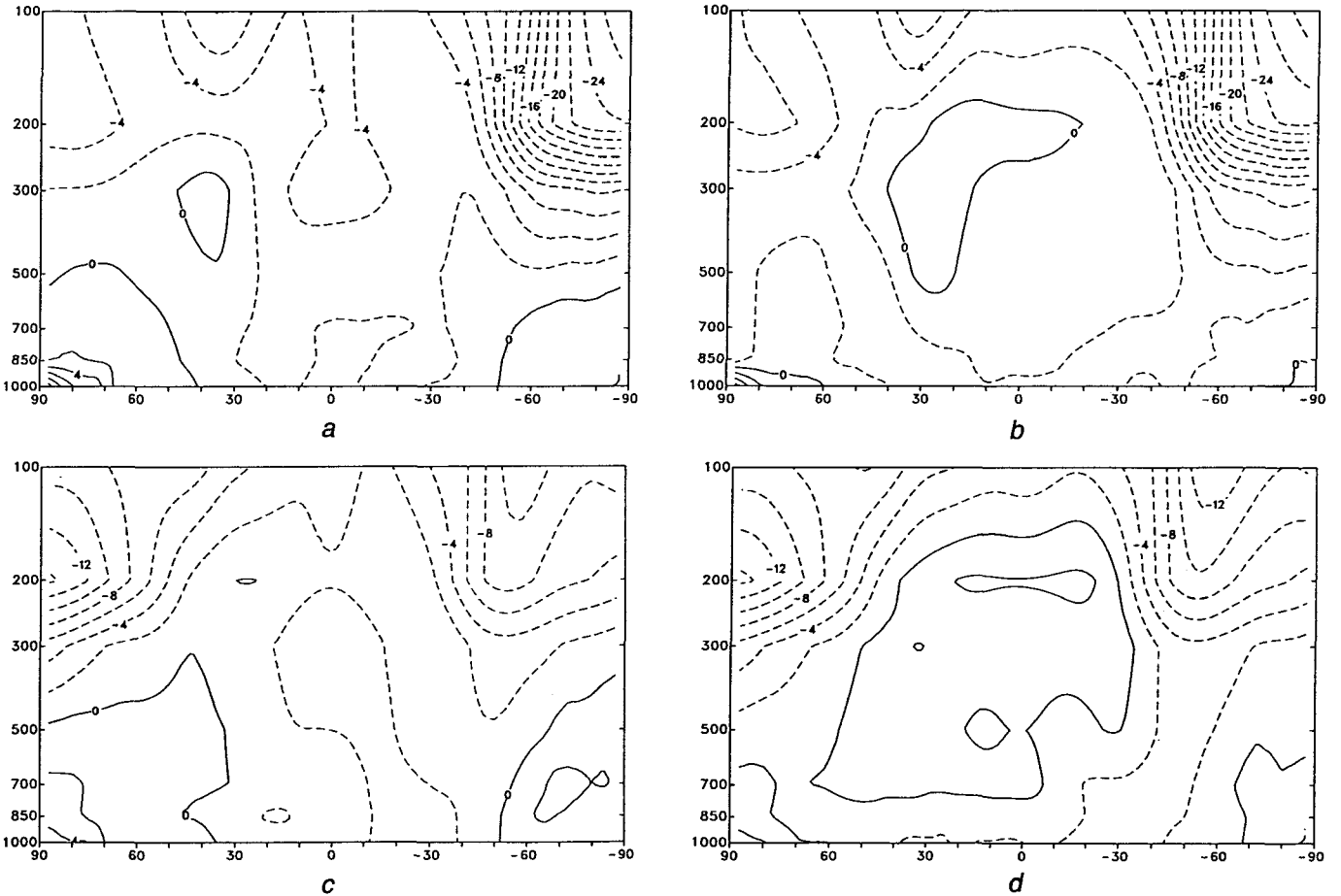

Fig. 9 Zonally averaged differences (deg C) between simulated and observed climatological temperature fields. Observed climatology is estimated from 10 years of ECMWF objectively analyzed fields. (*a*) Control, Dec.–Feb.; (*b*) CONV, Dec.–Feb.; (*c*) CONTROL, June–Aug.; (*d*) CONV, June–Aug.

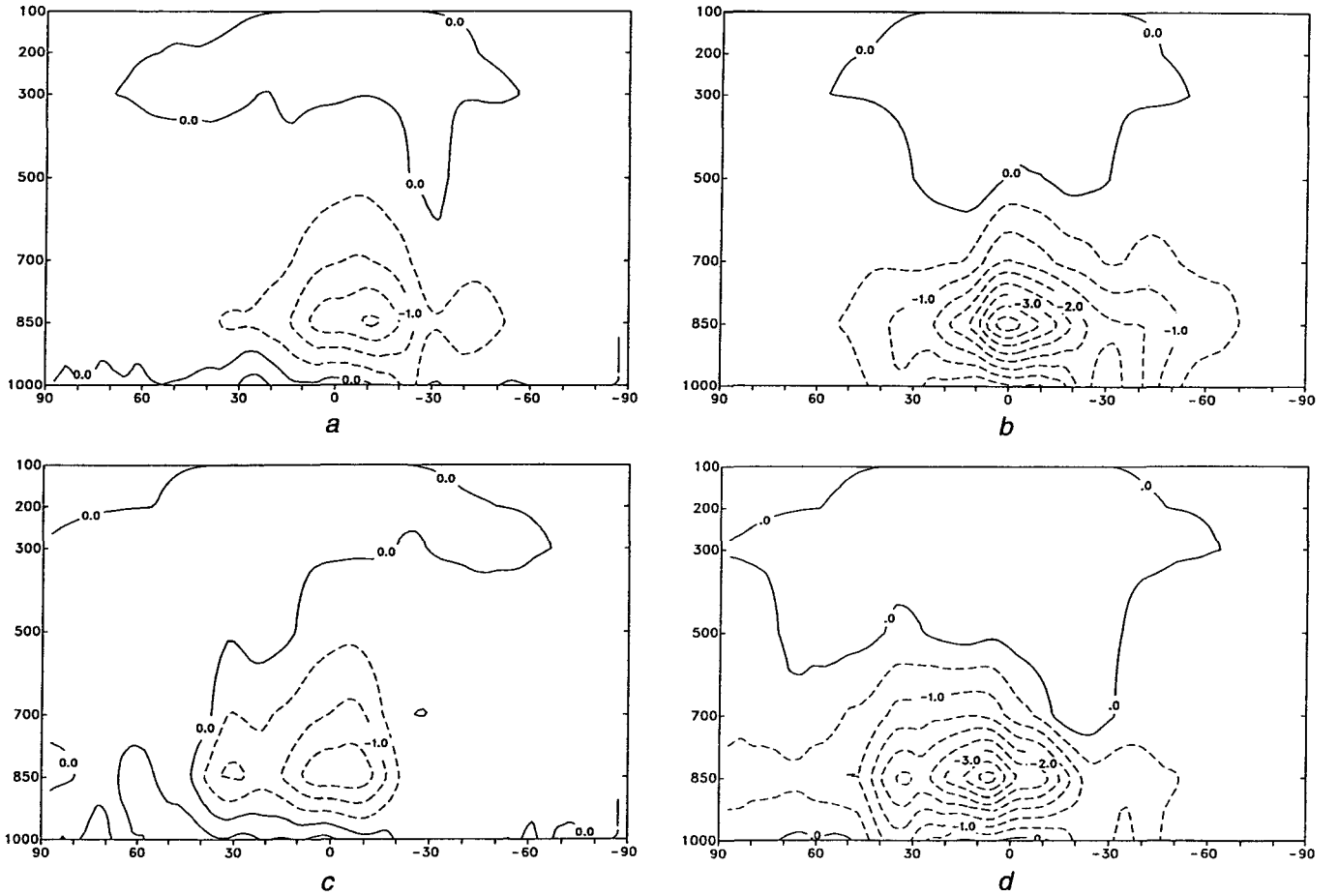

Fig. 10 As in Fig. 9 but for the specific humidity field. Units: g/kg.

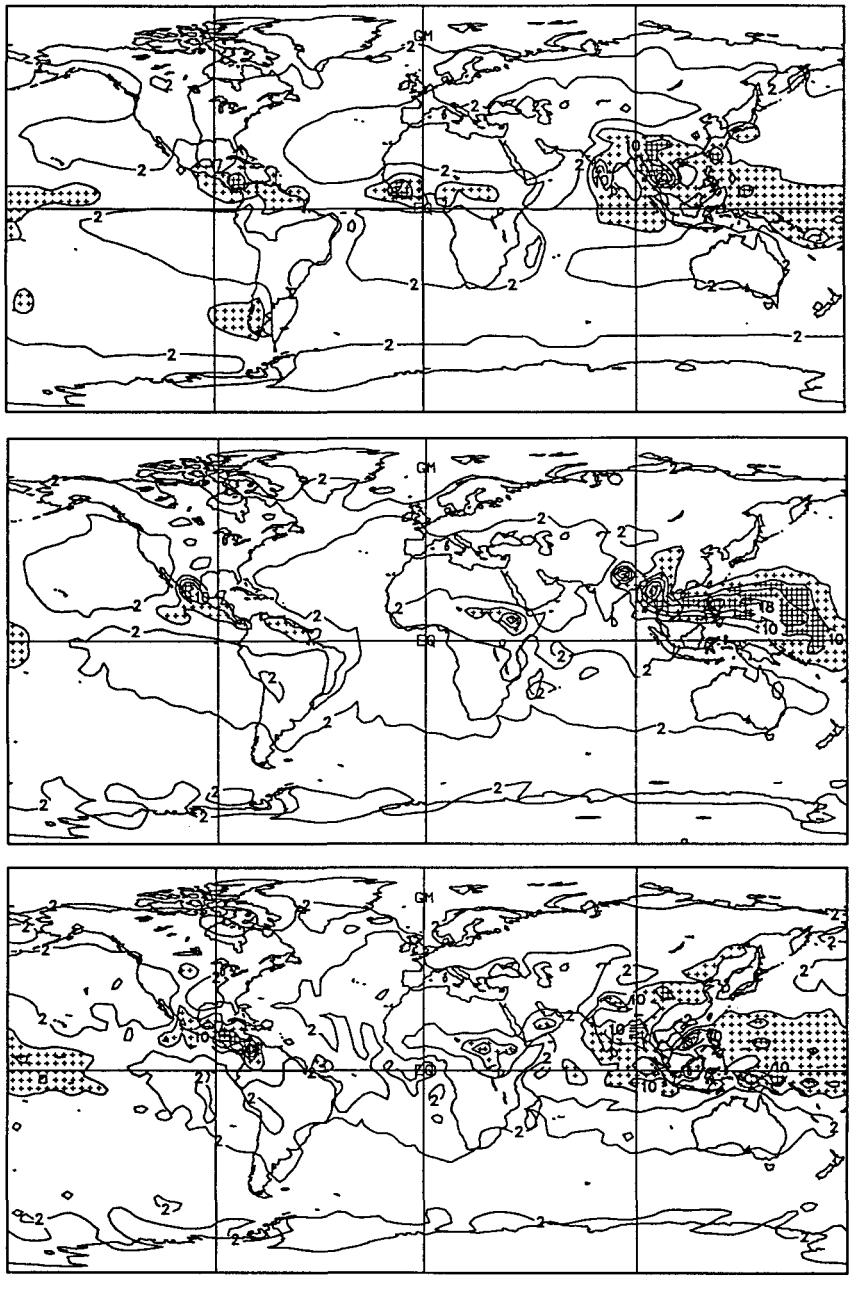

Fig. 11 Simulated and climatological (Jeager) precipitation fields. (*a*) Observed June–Aug.; (*b*) CONTROL June–Aug.; (*c*) CONV June–Aug.; (*d*) Observed Dec.–Feb.; (*e*) CONTROL Dec.–Feb.; (*f*) CONV Dec.–Feb. Units: mm/day.

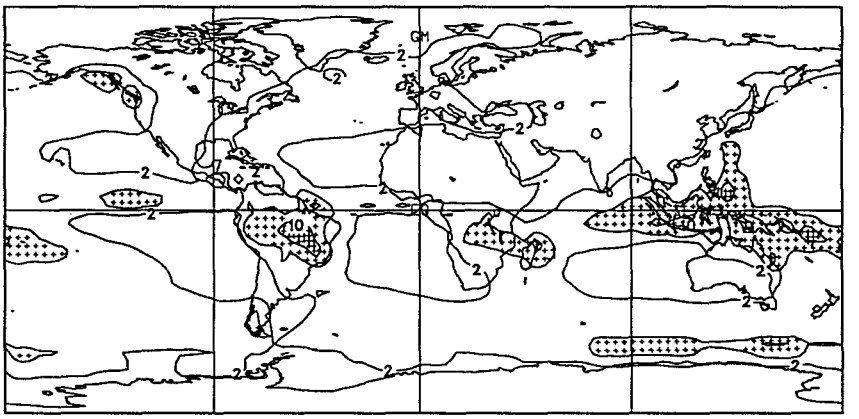

d

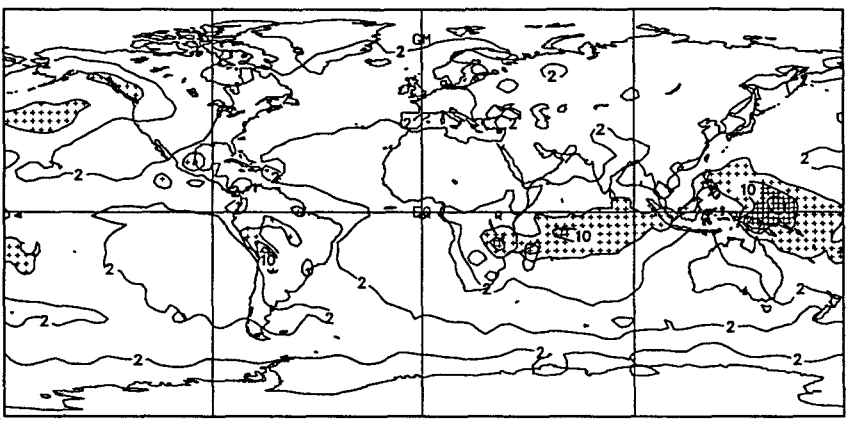

e

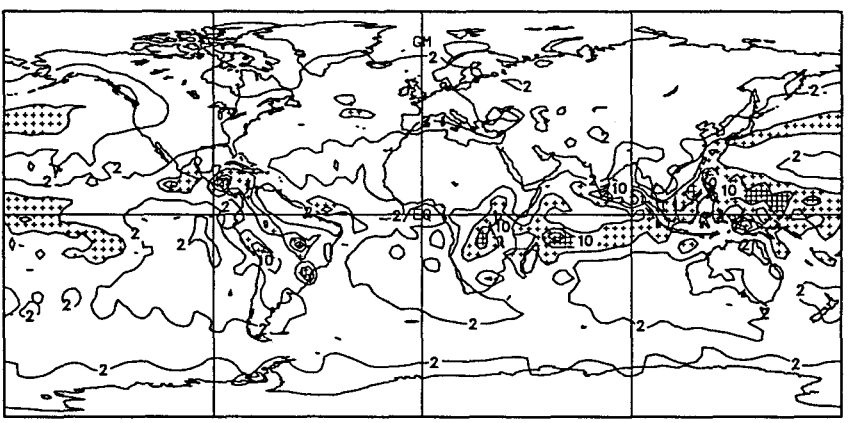

f

b *Precipitation and Tropical Circulation Patterns*

The main features of the climatological precipitation patterns are captured in both simulations (Figure 11). There are, however, pronounced local differences between the two simulations of this field. A particularly interesting difference is in the simulation of the Indian and Southeast Asian monsoon regime during the boreal summer. This regime is characterized by large amounts of precipitation over India and South-East Asia associated with the low-level jet that crosses the equator off the east coast of Africa and flows northeastward over the Arabian sea and eastward over India. Although both simulations reproduce the main features of this circulation regime, the CONTROL simulation has a deficit of precipitation over India and an excessive eastward and northward extension of the precipitation pattern over the southwestern Pacific ocean. These features are alleviated by introduction of the penetrative convection parameterization, although comparison with the observed climatological patterns suggests that there is still a deficit of precipitation over western India in the CONV simulation. This may in part be the result of inadequately resolving important topographic features such as the Western Ghat mountains.

The changes to summer monsoon simulations in these experiments are very similar to those of the single-season experiments discussed in greater detail by Zhang (1994). The model used in that study is a version of the CCC model with higher vertical resolution, a different land surface scheme, and with sea surface temperatures specified from climatological values. The monsoon circulation regime for a simulation made without any explicit parameterization of moist convection is compared to one made with the same penetrative convection scheme as was used in the present study. An interesting conclusion of that study is that simulations made with no explicit moist convection scheme are qualitatively similar to those made with the moist convective adjustment scheme of the CONTROL run in the present study. In both cases, the eastward extension of the monsoon precipitation pattern is associated with excessive westerly flow (not shown here for the CONTROL run) in the lower troposphere and excessive moisture convergence. These features are not present in the simulations made with the penetrative convection scheme.

c *Clouds, Radiation, and the Surface Energy Budget*

An important part of the simulated climate change resulting from introduction of the penetrative convection scheme is associated with the radiative response to changes in the spatial distribution of clouds and their optical properties. Although the globally averaged total fractional cloud cover is almost the same in both experiments (near 51% in all seasons), there are significant differences in the spatial distribution of cloudiness. Figure 12 shows the zonally averaged vertical distribution of the change in cloudiness for the summer and winter seasons. In general, introduction of the penetrative convection scheme results in substantial reduction of low cloud amounts, particularly in the tropics, and an associated increase in high cloud amounts.

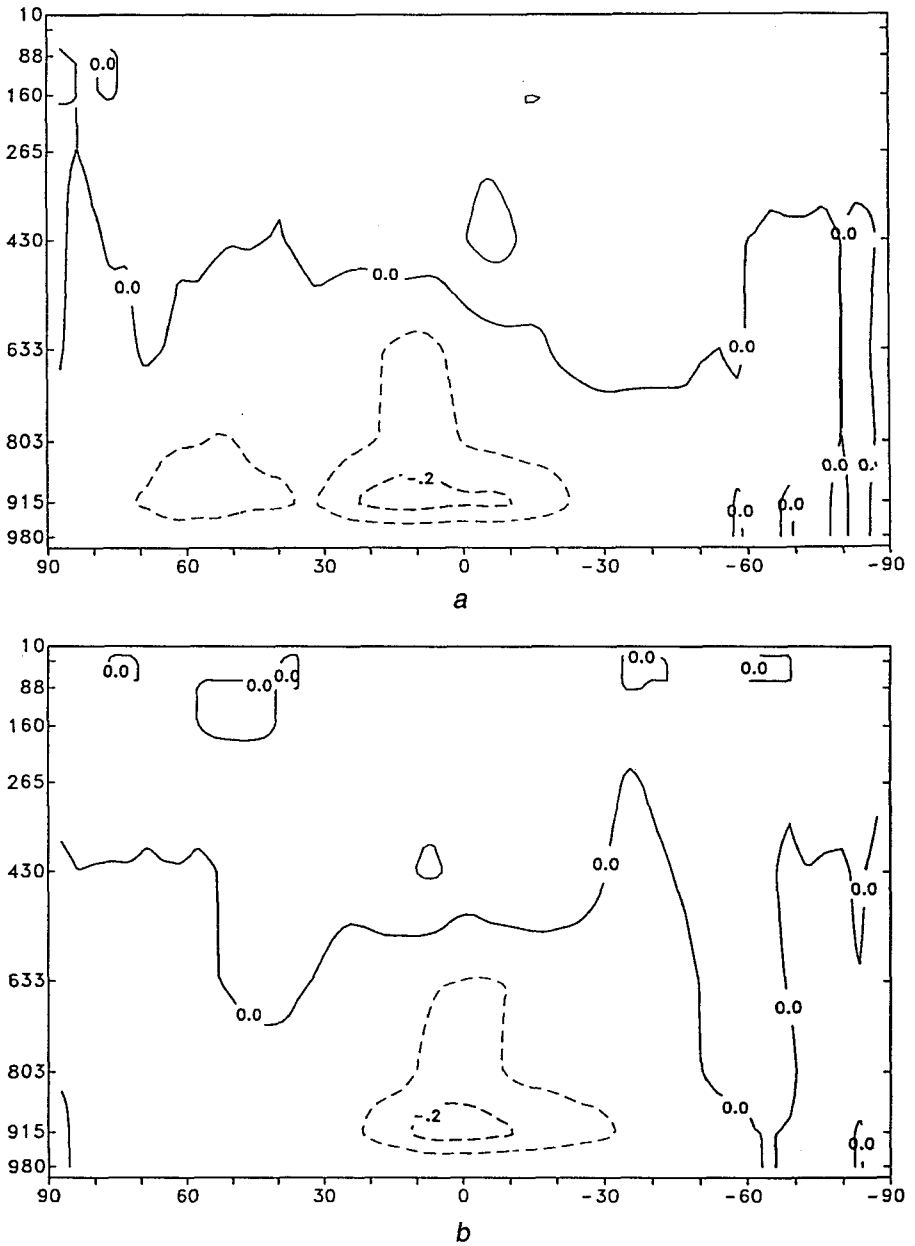

Fig. 12 Zonally averaged change in simulated cloudiness (CONV-CONTROL). (*a*) June–Aug.; (*b*) Dec.–Feb.

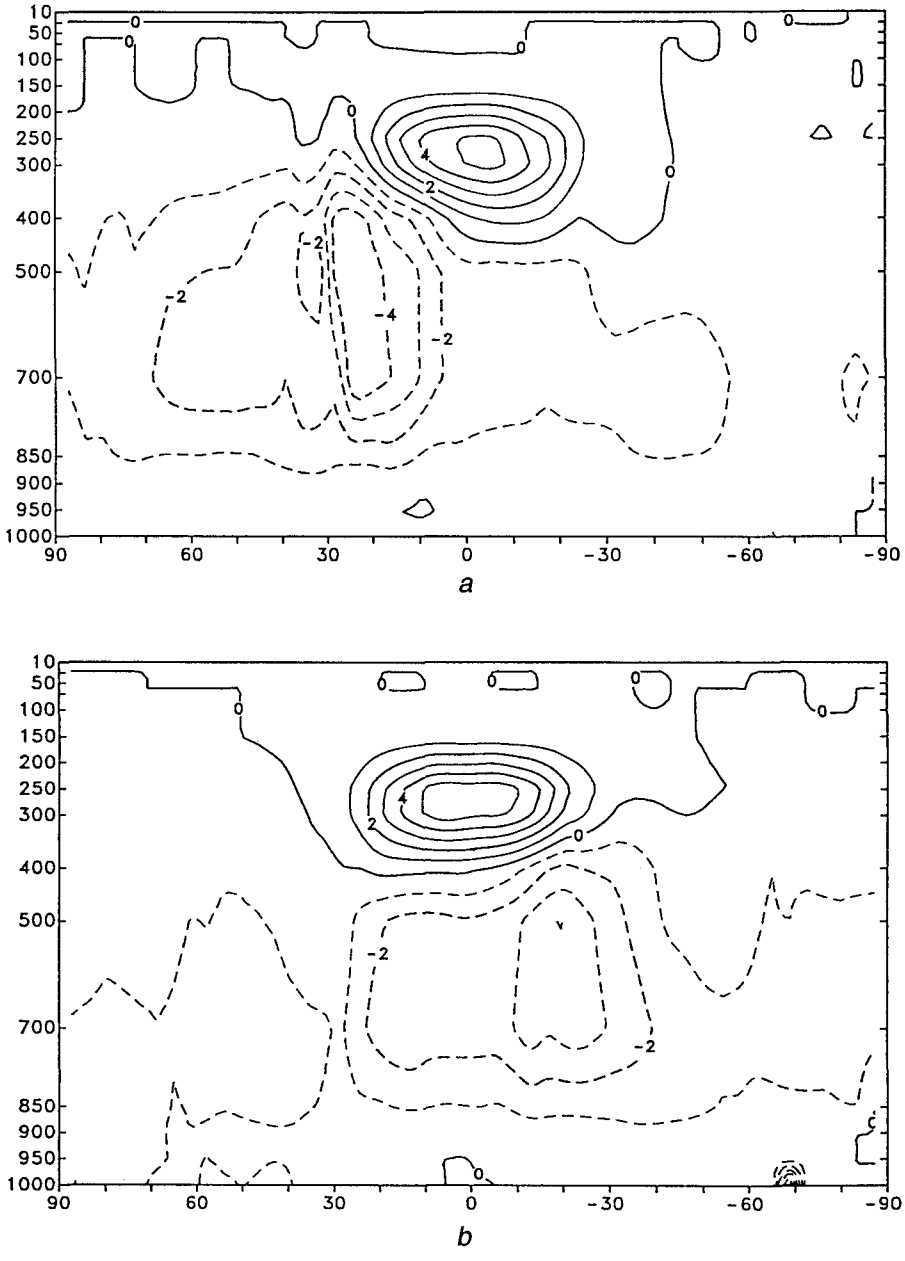

Fig. 13 As in Fig. 12 but for the representative optical depth.

As discussed by McFarlane et al. (1992), the optical properties of clouds are determined in the model as a function of the cloud liquid water content which, in turn, is parameterized in terms of the adiabatic water content that may occur with a specified amount of local lifting. Thus it varies with local conditions and allows changes in cloudiness to be accompanied by changes in the optical properties of the clouds. This is reflected, for example, in the changes in the zonally averaged representative cloud optical depth depicted in Figure 13. This quantity is defined as

$$[\tau] = [C\tau]/[C]$$

where τ is the local optical depth of a 100 mb thick cloudy layer and C is the local fractional cloud amount.

The changes in cloud amount and optical properties have important consequences for the radiation budget. This is illustrated for the boreal summer in Figure 14. The out-going long-wave radiation (OLR) is reduced as a consequence of the more abundant high clouds (Figure 14a). These clouds also reflect more solar radiation resulting in a general increase in the planetary albedo (Figure 14b). Although these changes have opposing effects on the net radiation at the top of the atmosphere, their combined effect is to reduce both the net incoming radiation in the summer hemisphere and the net outgoing radiation in the winter hemisphere (Figure 14c). Qualitatively similar effects are also found for the winter (December–February) season.

At the surface of the earth, the net radiative energy flux is generally downward at all but the high latitudes of the winter hemispheres. This downward net radiative flux is partially offset by the energy loss from the surface due to upward fluxes of sensible and latent heat associated with evaporation at the surface. The combined effect of these processes is to give a net downward flux of energy at the surface in the summer hemisphere and a net upward flux in the winter hemisphere.

Fig. 15, which depicts the changes (CONV-CONTROL), shows that introduction of the convection scheme results in generally increased magnitudes for the zonally averaged values of the individual flux terms. An exception is the sharply decreased net radiative flux at high latitudes in the summer hemispheres. This is due to the increased surface albedo associated with increased sea ice extent in the CONV simulation. Elsewhere the changes in sensible and latent heat fluxes tend to compensate those for the net radiative flux. The combined effect of these changes is reduced net downward flux at extra-tropical latitudes in the summer hemispheres and reduced net upward flux at high latitudes in the winter hemisphere.

The heat capacity of the land surface layer is small and there is no net flux of heat within the layer. Thus the seasonally averaged net flux at the surface is nearly zero over land surfaces. An exception may be found in high latitudes and/or over high terrain where a small net heat flux may be required to balance the latent heat

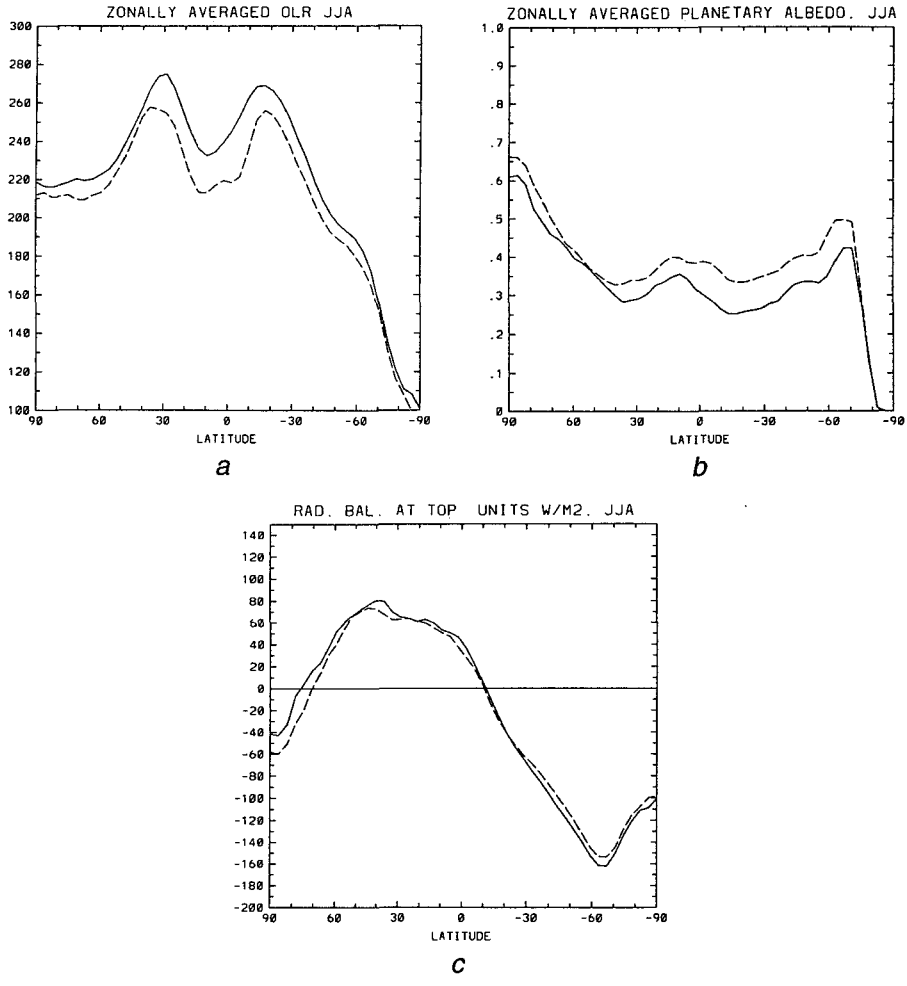

Fig. 14 Zonally averaged values of (*a*) Out-going long-wave radiation W/m^2, (*b*) Planetary albedo, (*c*) Net radiative flux at the top of the atmosphere W/m^2. Solid lines are the CONTROL simulation, dashed lines CONV.

exchange associated with freezing and thawing of soil moisture and melting of snow. These considerations apply also to the CONV simulation. Thus differences in the net surface flux are also generally small over land surfaces.

In contrast, in regions occupied by open ocean and sea ice, the net surface flux is of significant magnitude and spatially variable. In these regions, the local net energy gain/loss due to surface fluxes is balanced by changes of the storage of thermal energy in the sub-surface layers, sub-surface heat transport and, where present, freezing or melting of sea ice and snow. The sub-surface heat flux is specified

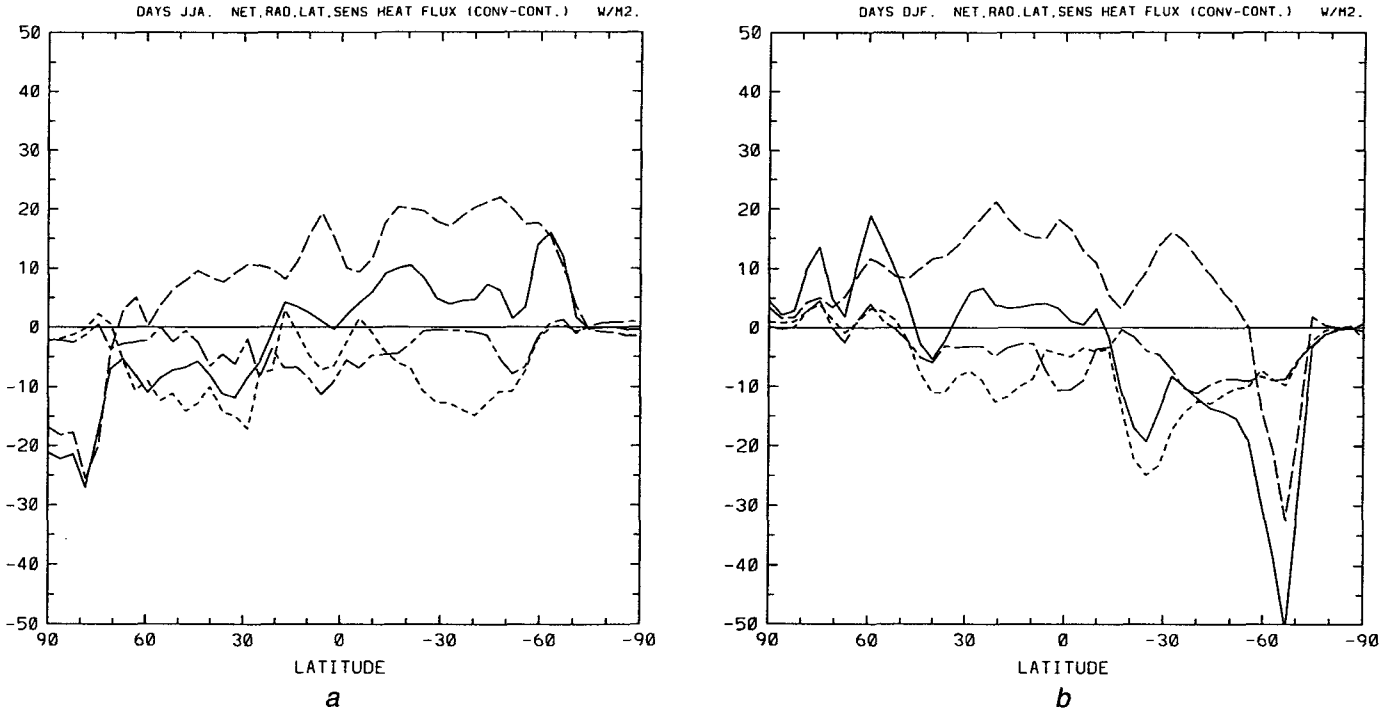

Fig. 15 Zonally averaged differences for terms in the surface energy balance for the CONTROL simulation. (*a*) June–Aug. (*b*) Dec.–Feb. Solid: net (positive downward) energy flux at the surface. Long dashed: net radiative flux. Short dashed: Latent heat flux due to evaporation from the surface. Long-short dashed: Sensible heat flux. Units: W/m^2.

under the sea ice and within the 50 m thick oceanic mixed layer in both simulations. As discussed in MBBL, these vary on a monthly time scale in such a way as to ensure that the evolution of sea surface temperatures and sea ice in the CONTROL simulation is acceptably close to observed climatology throughout the annual cycle. This sub-surface flux specification is unchanged for the CONV simulation. Thus the differences in net surface flux imply that for this simulation, there is an energy flux imbalance for the surface layer. Maintenance of a climatological equilibrium in which sea surface temperatures and sea ice extent remain close to observed values throughout the annual cycle is not possible in these circumstances.

Figure 16, which depicts the ensemble mean surface temperature differences between the two simulations, shows that while the CONV simulation is warmer over some parts of the land surface in the tropics, it is generally colder elsewhere. Although the largest cooling is in higher latitudes over land and sea ice areas in the winter hemispheres, there is also significant cooling elsewhere, particularly at high latitudes in the summer hemisphere. The substantial heat capacity of the oceanic surface layer ensures that surface temperatures in those regions respond relatively slowly to the energy flux imbalance implied by the difference fields shown in Fig. 16. Thus the CONV simulation was not in equilibrium when it was terminated. The globally averaged monthly mean values of the surface air temperature for the last two years are less than the corresponding ensemble mean values for the CONTROL simulation, suggesting that it was drifting toward a generally cooler climatic state.

7 Discussion and conclusions

The bulk cumulus parameterization presented in this paper is simple enough to be relatively easily implemented in a GCM. It is designed to represent mainly the effects of deep convection and does retain the important features of penetrative convection schemes of this type. The simple column tests presented show that the convection scheme comes into equilibrium with imposed forcing. Although the nature of the equilibriated state is sensitive to the specification of the various disposable parameters, particularly the adjustment time scale and the initial downdraft mass flux, the temporally averaged features of the equilibrium states obtained with the new cumulus scheme are broadly similar. In general, the effect of the new parameterization scheme is significantly different from that of the moist convective adjustment scheme currently used in the second generation version of the CCC GCM. In particular, the radiative-convective equilibrium obtained using the convective adjustment scheme yields substantially colder temperatures in the upper troposphere. The regime is also somewhat less moist in that region but more so in the lower troposphere.

A limitation of these simple column tests is that they do not allow some of the more important components of the large-scale forcing to respond to convective heating. However, the full GCM climate simulations corroborate many of the results of the column tests. In particular, it is shown that the cold anomaly in the tropics for

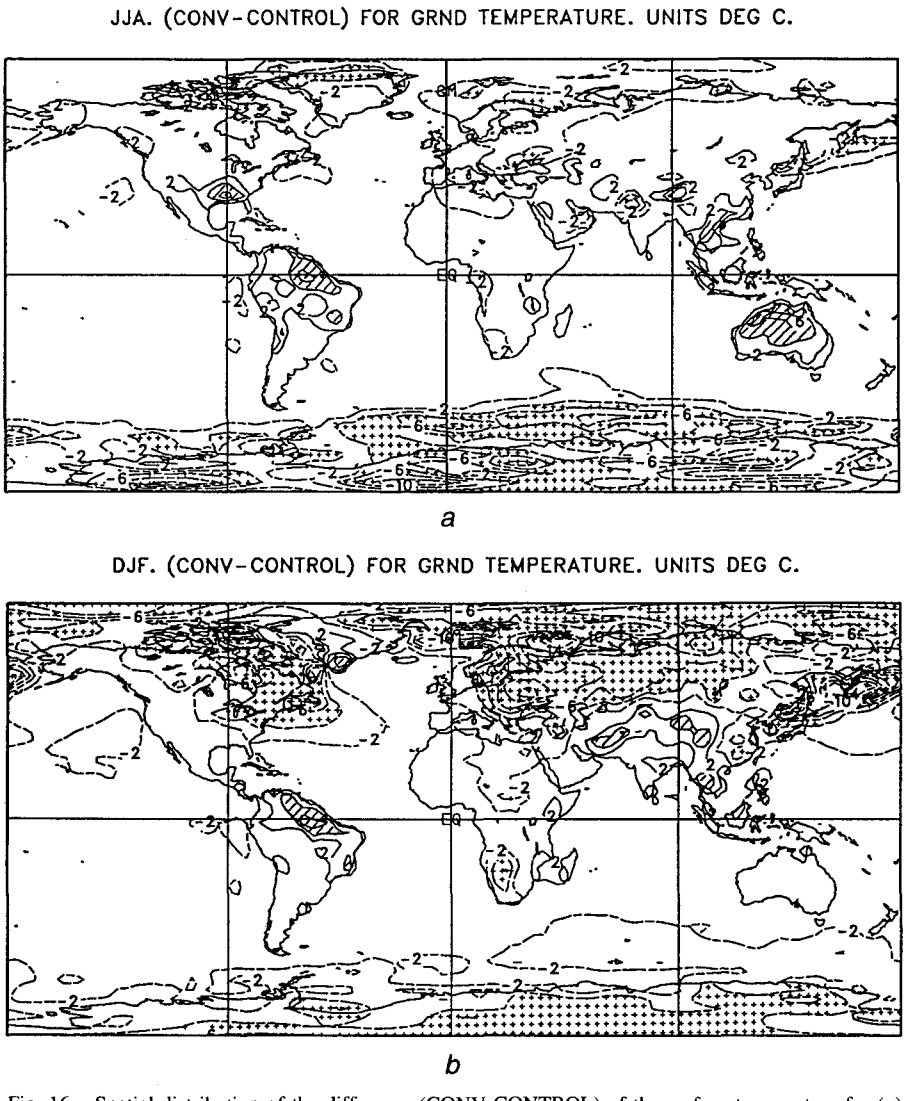

Fig. 16 Spatial distribution of the difference (CONV-CONTROL) of the surface temperature for (*a*) June–Aug.; (*b*) Dec.–Feb. Hatched regions have values larger that 4C, shaded less than −4C.

the CONTROL simulation is removed by replacing the moist convective adjustment scheme with the new cumulus ensemble scheme. This change is accompanied by drying in the lower troposphere and moistening in the upper troposphere.

An interim specification of the disposable parameters is made for the version of the cumulus parameterization scheme used in the CONV simulation. The choice of 2 hours for the adjustment time used in the GCM experiment is based on results

from a few monthly simulation tests which tend to suggest that it is somewhat optimal in the sense that it ensures that the precipitation regime in the tropics is predominantly convective while preventing excessive stabilization due to the choice of a value which is too small. Similarly short tests of the sensitivity to specification of the initial downdraft mass flux suggest that the GCM simulations are somewhat less sensitive to variations in this parameter than are the column model simulations. However, use of the "strong downdraft" version does reduce somewhat the lower troposphere drying (relative to the CONTROL simulation). This is consistent with the results of the column model simulations.

A significant reduction in lower tropospheric cloudiness and a slight increase of cloud cover in the upper troposphere accompany the changes in thermodynamic structure. These changes are also accompanied by important changes in cloud optical properties and consequently of the radiation budget. The planetary albedo is increased and out-going longwave radiation is reduced in the CONV simulation. Although these changes have opposite effects on the energy balance, there is a general reduction of the magnitude of the net radiative flux at the top of the atmosphere.

These are also significant changes in the energy balance at the surface. The net downward radiative flux is increased in tropical and middle latitudes but sharply decreased in high latitudes of the summer hemisphere. This reduction is associated with the albedo change that accompanies increased sea-ice cover. The increased downward radiative flux in the tropics and middle latitudes is partially compensated by increased upward fluxes of sensible and latent heat. Both the net surface flux and changes to it are small over land. However, over oceanic regions, the changes are more complicated and include areas of substantial net increases and decreases. Since these changes are not accompanied by changes in the sub-surface flux in the mixed layer or undersea ice, sea surface temperatures and sea-ice mass and extent change as well.

It is of interest to compare these results to those presented by Washington and Meehl (1993). They show that addition of a penetrative convection scheme to a version of the NCAR CCM2 that includes a 50 m thick oceanic mixed layer results in an increase in upper tropospheric cloud with an associated enhancement of the planetary albedo. This was also accompanied by an increase in the global mean surface temperature even though there was a net increase in the rate of heat loss from the surface due to a substantial increase in surface evaporation. Thus the reduction in solar radiation at the surface due to increased reflectivity of cirrus clouds was not sufficient to inhibit enhancement of the greenhouse effect. The authors show, however, that increasing the albedo of cirrus clouds that occur over warm pools of the ocean results in smaller global mean increases in surface temperature and evaporation. It is also found that introduction of penetrative convection alone enhances the global mean surface warming due to doubling of CO_2 but allowing the additional feed-back associated with the enhancement of cirrus cloud albedos over the warm ocean surface nearly offsets this. This is associated with a reduced

radiative input at the surface, which is balanced mainly by a reduction in the heat loss due to evaporation.

These results are consistent with those of Boer (1993), who showed that the negative feedback associated with increased reflectivity of cirrus clouds plays a significant role in determining the equilibrium response to doubling of CO_2 as simulated with the CCC GCM. In particular, it results in a significantly smaller increase in surface evaporation than is typically found in earlier simulations of this type. Although cloud cover decreases in the tropics in the doubled CO_2 simulation, the optical thickness of upper tropospheric clouds increases in a manner similar to that depicted in Fig. 15. It should be noted that the version of the model used for the doubled CO_2 experiment is identical in its physical parameterization to that used here for the CONTROL run (Boer et al., 1992).

Although the responses of individual components in the CONV experiment are qualitatively similar to that found by Washington and Meehl (1993), and somewhat different from what is found for a doubling of CO_2, the net effect is slight cooling rather than warming of the surface. This is predominantly associated with enhanced evaporation rather than reduced solar input. This effect is, not surprisingly, sensitive to features of the convection scheme and the way that it couples to other parameterized processes in the boundary layer. The version of the penetrative convection scheme used in this simulation tends to be biased toward deep convection, which acts to dry and cool the boundary layer. Although these effects are partially balanced by increased surface evaporation and sensible heat flux, a slight reduction of the low level moisture also results, in contrast to the finding of Washington and Meehl (1993).

Although introduction of the penetrative convection scheme corrects some significant biases in climate simulations, the changes in the radiation budget that give rise to the drift toward a cooler surface are an undesirable feature of the response. Correcting these defects requires modifications of other parameterizations also and is the subject of current work. Apart from this, the scheme as used here is not completely satisfactory in its representation of shallow convection. This may be reflected to some extent in the enhanced dryness of the lower troposphere in the CONV simulation, although it is also somewhat reduced when stronger downdrafts are used, and is also sensitive to vertical resolution and boundary-layer mixing. Neverthelesss, it may be desirable to incorporate an explicit shallow convection scheme to complement and/or replace, the penetrative scheme in circumstances where shallow convection is expected to occur predominantly, as is done for example in the Betts-Miller scheme as used by Slingo et al. (1994).

A representation of the vertical momentum transfer by cumulus clouds, similar in form to that proposed by Zhang and Cho (1991), has also been designed and tested in seasonal GCM simulations. That work is reported separately (Zhang and McFarlane, 1995).

Appendix: Determining entrainment rates

To determine $\lambda_D(z)$, we consider a cloud type with entrainment rate λ. If clouds are assumed in a steady state, the moist static energy h_u of the updraft satisfies

$$\frac{\partial h_u}{\partial z} + \lambda(h_u - h) = 0. \tag{A1}$$

Assuming that the updraft moist static energy is equal to the environmental (approximately the large-scale mean) value, h_b, at the detrainment level, the updraft air is saturated and has the same temperature as the environmental air ($h_u \cong h^*$), if follows from the above equation that

$$h_b - h^*(z) = \lambda_D(z) \int_{z_b}^{z} (h_u - h) dz'. \tag{A2}$$

In principle, eqs. (A1) and (A2) can be used to determine $\lambda_D(z)$ by iteration. A Newton-Raphson procedure can be used effectively provided a reasonable first guess is supplied for h_u, or alternatively of $\lambda_D(z)$. The procedure outlined here utilizes reversion of series to derive a high-order Newton-Raphson scheme that provides a first-guess estimate that is often sufficiently accurate that further refinement by iteration is not required.

The updraft moist static energy can be expanded in a Taylor series in λ as

$$h_u(\lambda, z) = h_u(0, z) + \Sigma_n \left(\frac{1}{n!}\right) \left.\frac{\partial^n h_u}{\partial \lambda^n}\right|_{\lambda=0} \lambda^n. \tag{A3}$$

The first term on the right-hand side of (A3) is h_b and the derivatives with respect to λ can be obtained by noting that h_b is independent of λ and using (A1) to show that

$$\left.\frac{\partial^n h_u}{\partial \lambda^n}\right|_{\lambda=0} = (-1)^n n! I_n \tag{A4}$$

where I_n is the nth order integral

$$I_n = \int_{z_b}^{z} \cdots (h_b - h) dz^{(n)}. \tag{A5}$$

Substitution of (A3), (A4), and (A5) into (A2) and applying reversion of series yields:

$$\lambda = \Delta + \frac{I_2}{I_1} \Delta^2 + \frac{(2I_2^2 - I_1 I_3)}{I_1^2} \Delta^3 + \cdots \tag{A6}$$

where

$$\Delta = \frac{h_b - h^*}{I_1}.$$

The first three terms of (A6) are often sufficient to provide an accurate estimate of $\lambda_D(z)$.

References

ARAKAWA, A. and W.H. SCHUBERT. 1974. Interaction of cumulus cloud ensemble with the large-scale environment, Part I. *J. Atmos. Sci.* **31**: 674–701.

BETTS, A.K. 1976. The thermodynamic transformation of the tropical subcloud layer by precipitation and downdrafts. *J. Atmos. Sci.* **33**: 1008–1020.

———. 1986. A new convective adjustment scheme. Part I: Observational and theoretical basis. *Quart. J. Roy. Meteorol. Soc.* **112**: 677–691.

BOER, G.J.; N.A. MCFARLANE and M. LAZARE. 1992. Greenhouse gas-induced climate change simulated with the CCC second-generation general circulation model. *J. Climate* **5**: 1045–1077.

———. 1993. Climate change and regulation of the surface moisture and energy budgets, *Clim. Dyn.* **8**: 225–239.

BOLTON, D. 1990. The computation of equivalent potential temperature. *Mon. Wea. Rev.* **108**: 1046–1053.

CHO, H.R. 1977. Contribution of cumulus life-cycle effects to the large-scale heat and moisture budget equations. *J. Atmos. Sci.* **34**: 87–97.

EMANUEL, K.A. 1991. A scheme for representing cumulus convection in large-scale models. *J. Atmos. Sci.* **48**: 2313–2335.

FRANK, W.M. and J.L. MCBRIDE. 1989. The vertical distribution of heating in AMEX and GATE cloud clusters. *J. Atmos. Sci.* **46**: 3464–3478.

GREGORY, D.R. and P.R. ROWNTREE. 1990. A mass flux convective scheme with representation of cloud ensemble characteristics and stability dependant closure. *Mon. Wea. Rev.* **118**: 1483–1506.

GRELL, G.; Y.-H. KUO and J.R. PASCH. 1991. Semi-prognostic tests of cumulus parameterization schemes in the middle latitudes. *Mon. Wea. Rev.* **119**: 5–31.

JOHNSON, R.H. 1976. The role of convective-scale precipitation downdrafts in cumulus and synoptic-scale interactions. *J. Atmos. Sci.* **33**: 1890–1910.

———. 1978. Cumulus transports in a tropical wave composite for phase III of GATE. *J. Atmos. Sci.* **35**: 484–494.

———. 1980. Diagnosis of mesoscale motions during phase III of GATE. *J. Atmos. Sci.* **37**: 733–753.

KNUPP, K.R. 1987. Downdrafts within High Plains cumulonimbi, Part I: General kinematic structure. *J. Atmos. Sci.* **44**: 987–1008.

KUO, H.-L. 1965. On formation and intensification of tropical cyclones through latent heat release by cumulus convection. *J. Atmos. Sci.* **22**: 40–63.

———. 1974. Further studies of the properties of cumulus convection on the large scale flow. *J. Atmos. Sci.* **31**: 1232–1240.

LEWIS, J.M. 1975. Tests of the Ogura-Cho model on a prefrontal squall line case. *Mon. Wea. Rev.* **103**: 764–778.

LORD, S.J. 1982. Interaction of a cumulus cloud ensemble with large-scale environment. Part III: Semi-prognostic test of the Arakawa-Schubert cumulus parameterization. *J. Atmos. Sci.* **39**: 88–103.

MANABE, S.; J. SMAGORINSKY and R.F. STRICKLER. 1965. Simulated climatology of a general circulation model with a hydrologic cycle. *Mon. Wea. Rev.* **93**: 769–798.

MCFARLANE, N.A.; G.J. BOER, J.-P. BLANCHET and M. LAZARE. 1992. The Canadian Climate Centre second generation circulation model and its equilibrium climate. *J. Climate* **5**: 1013–1044.

MOORTHI, S. and M.J. SUAREZ. 1992. Relaxed Arakawa-Schubert: A parameterization of moist convection for general circulation models. *Mon. Wea. Rev.* **120**: 978–1002.

OGURA, Y. and H.-R. CHO. 1973. Diagnostic determination of cumulus cloud populations from observed large-scale variables. *J. Atmos. Sci.* **30**: 1276–1286.

SLINGO, J.N.; M. BLACKBURN, A. BETTS, R. BRUGGE, K. HODGES, M. MILLER, L. STEENMAN-CLARK and J. THUBURN. 1994. Mean climate and transience in the tropics of the UGAMP GCM: Sensitivity to convective parameterization. *Q.J.R. Meteorol. Soc.* **120**: 881–922.

TIEDTKE, M. 1989. A comprehensive mass flux scheme for cumulus parameterization in large-scale models. *Mon. Wea. Rev.* **117**: 1779–1800.

WASHINGTON, W.M. and G.A. MEEHL. 1993. Greenhous sensitivity experiments with penetrative cumulus convection and tropical cirrus cloud effects. *Clim. Dyn.* **8**: 211–223.

YANAI, M.; S.K. ESBENSEN and J.-H. CHU. 1973. Determination of bulk properties of tropical cloud

clusters from large-scale heat and moisture budgets. *J. Atmos. Sci.* **30**: 611–627.

———; J.-H. CHU and T.E. STARK. 1976. Response of deep and shallow tropical cumuli to large-scale processes. *J. Atmos. Sci.* **33**: 976–991.

ZHANG, G.J. and N.A. MCFARLANE. 1991. Convective stabilization in midlatitudes. *Mon. Wea. Rev.* **119**: 1915–1928.

——— and H.R. CHO. 1991. Parameterization of the vertical transport of momentum by cumulus clouds. Part II: Application. *J. Atmos. Sci.* **48**: 2448–2457.

———. 1994. Effects of cumulus convection on the simulated monsoon circulation in a general circulation model. *Mon. Wea. Rev.* **122**: 2022–2038.

——— and N.A. MCFARLANE. 1995. Role of convective-scale momentum transport in climate simulations. *J. Geophys. Res.* **100**: 1417–1426.